

Anatomically Accurate Motorized Shoulder Model with Scapula Movement

Ella Deane, Danielle LaBlanc, Bailey Savage, and Shawna Winters



Worcester Polytechnic Institute

Major Qualifying Project

Professor Fiona Levey

April 15, 2022

This report represents the work of one or more WPI undergraduate students submitted to the faculty as evidence of completion of a degree requirement. WPI routinely publishes these reports on its site without editorial or peer review.

Abstract

Medical education and shoulder injury research would benefit from an anatomically correct physical model that includes the kinematic accuracy of scapulohumeral rhythm. Our model's defining feature is the inclusion of relative scapular movement, which is not found in existing physical models due to the complexity of the shoulder joint. We engineered a full-scale, anatomically accurate model with linearized muscle attachments that replicates motion of the shoulder bones during abduction using a motorized activation system. The model abducts the humerus from rest to 60° and repeatedly returns the scapula to within 5% of the initial position. Our model consistently achieved 1° of scapular rotation for every 3° of humeral abduction, which is within 33% of the average anatomical scapulohumeral ratio. We expect this model to evolve into an innovative commercial product with additional muscles and more realistic soft tissue attachments that would improve the model's mechanics and increase its range of motion.

Acknowledgements

Our team would like to thank several key people for their contributions to the success of our project. We would like to thank Dominick Gravante for his assistance with the robotics aspects of our project and generosity. We would also like to thank Noah Roberts for his help with the programming of our model. We would like to thank Dr. Crispin Weinberg for providing us with the STL files for our modeled bones. We would like to thank John Kennedy for his daily support and endless supply of chocolate. Finally, we would like to thank our wonderful advisor Fiona Levey for her guidance, support, and expertise.

Table of Contents

Abstract.....	1
Acknowledgements.....	2
Introduction.....	10
Literature Review.....	11
Anatomy and Kinematics.....	11
General Overview of Anatomy.....	11
Bones.....	12
Musculature.....	14
Joints and Ligaments.....	16
Common Shoulder Injuries.....	18
Descriptions of Common Injuries.....	18
Acromioclavicular Separation.....	18
Anterior and Posterior Instability.....	19
SLAP Tears.....	20
Clavicle Fracture.....	21
Rotator Cuff Injury.....	21
Existing Shoulder Models.....	22
Realistic Educational Models.....	22
Design Software.....	23
Imaging and Virtual Modeling Techniques.....	23
Leaders in the Field.....	24
3D Printing Biomedical Models.....	24
FEA Models.....	28

Replication and Activation Techniques	30
Cable-Winch Actuation.....	30
Pneumatic Artificial Muscles	31
Literature Review Conclusion	33
Methodology.....	34
Short-term Project Goals.....	34
Design and Construction Goals.....	34
Model Movement and Positioning Goals	34
Long-Term Goals for Future MQPs:.....	34
Model Movement and Positioning Goals.....	35
Goal One: Accurate Positioning of the Scapula	35
Goal Two: Achieve Desired Range of Motion.....	36
Goal Three: Accurate Relative Motion.....	38
Design Concepts: Overall Rig Structure.....	39
Design One: Mechanical Scapulothoracic Joint.....	39
Scapulothoracic Joint Design	40
Glenohumeral Joint.....	41
Sternoclavicular Joint	42
Design Two: Physical Rib Cage Design	43
Final Structural Rig Design	45
Manipulated Rib Cage Model.....	46
Sternoclavicular Joint.....	48
Glenohumeral Joint	51
Selection of Soft Tissue Groups.....	52
Ligaments	52

5 Muscle Groups	54
Stationary Motor Mounting Systems	54
Free Standing Motor Mounting Systems	56
Design One: Nema 17 and Worm Gearbox	56
Design Two (Final): Planetary Gearbox Nema 17 Stepper Motor	58
Manufacturing and Material Selection.....	59
Bone Modeling.....	59
Rig Assembly	64
Replication of Muscles and Ligaments	67
Material Selection	67
Ligaments	68
Muscles	70
Actuation System Implementation.....	71
Motor Selection	71
NEMA Motor Tests and Selection	73
Stationary Motor Mounting Systems.....	74
Humerus Motor Mounting Systems.....	75
Completed Model.....	75
Motor Circuitry and Motion Programming.....	76
Testing.....	78
Results.....	79
Goal One: Accurate Positioning of the Scapula	79
Goal Two: Achieve Desired Range of Motion.....	81
Goal Three: Accurate Relative Motion	82
Discussion	84

Conclusion and Recommendations.....	85
Broader Impact.....	86
Engineering Ethics	86
Social and Global Impact	87
Environmental Impact	88
Economic Impact.....	88
Appendices.....	89
Appendix A: Anatomical definitions/terms	89
Appendix B. Schematics for Soft Tissue Attachments	93
Appendix C: Potential Soft Tissue Material Options.....	105
Appendix D: Stepper Motor Specifications	110
References.....	112

List of Figures

Figure 1: Image of the human shoulder.....	13
Figure 2: Posterior view drawing of the bones of the shoulder girdle.....	14
Figure 3: Posterior view drawing of the scapula.....	14
Figure 4: Anterior grouping of the shoulder girdle muscles.....	17
Figure 5: Posterior grouping of the shoulder girdle muscles.....	18
Figure 6: Core movements of the shoulder.....	19
Figure 7: Image depicting AC joint anatomy.....	21
Figure 8: Image of Rockwood Classification of AC Joint Separations.....	22
Figure 9: Image of anterior and posterior dislocation of the shoulder.....	23
Figure 10: MRI image of healthy shoulder.....	24
Figure 11: Image depicting a broken collarbone.....	24
Figure 12: Image of healthy rotator cuff anatomy.....	25
Figure 13: Example model of right shoulder girdle created by Monash University.....	29
Figure 14: “Deluxe Functional Shoulder Joint Model” by 3B Scientific.....	30
Figure 15: “Functional Model of the Shoulder Joint” by SOMSO.....	30
Figure 16: Shoulder model created by Almeida-Galárraga et al.....	31
Figure 17: Cable-sheath setup with stiff tube sheath.....	34
Figure 18: Example relaxed non-pressurized and activated pressurized McKibben muscle.....	35
Figure 19: Example project that was built using grouped McKibben muscles.....	36
Figure 20: Image of scapular movements from the back, side, and top view.....	39
Figure 21: Image of scapular movements range of motion from the back, side, and top view....	39
Figure 22: Overview of abduction and adduction.....	40
Figure 23: Scapulohumeral rhythm during abduction and adduction.....	41
Figure 24: Visual representation of the “setting phase” and the relationship between the glenohumeral joint and scapula during arm movements.....	42
Figure 25: Sketch of Design Iteration One.....	43
Figure 26: Sketches of top, front, and side view of scapulothoracic joint.....	44
Figure 27: Sketches of top, front, and side view of the unique slot feature representing the scapulothoracic joint.....	44

Figure 28: Sketch of glenohumeral joint design.....	45
Figure 29: Ball joint linkage from McMaster-Carr.....	45
Figure 30: Isolated sketch of sternoclavicular joint design.....	46
Figure 31: Top view and side view of drawing for a rib cage design concept.....	47
Figure 32: 3D full-scale computer model of rib cage design concept.....	48
Figure 33: Front and back view of model true to scale.....	49
Figure 34: Left and right view of the model true to scale.....	49
Figure 35: Front and side views of full shoulder rig assembly.....	49
Figure 36: Front and right-side view of rib connections.....	51
Figure 37: Top view sketch of sternoclavicular joint design.....	53
Figure 38: Image on left is an “x-ray” view of full shoulder model design and image on right shows the plywood and support structure with the isolated clavicle.....	53
Figure 39: Clavicle and plywood attachments.....	54
Figure 40: Model from a 2019 study that focuses on kinematically uncoupled movement of the scapula.....	55
Figure 41: Anterior view of the glenohumeral ligaments that aid in humerus stability.....	56
Figure 42: First stationary motor mount designed to secure a single Nema 17 stepper motor to the top of the t-slot beam.....	58
Figure 43: Second stationary motor mount designed to secure a single Planetary Gearbox Nema 17 stepper motor to the top of the t-slot beam.....	58
Figure 44: Two-part block with the humerus subtracted from the middle.....	59
Figure 45: First design iteration in which the Nema 17 stepper motor sits upside down in the mount with the shaft directly inserted into a worm gearbox.....	60
Figure 46: Exposed view of the gearbox with a worm gear and worm wheel in its casing.....	60
Figure 47: Assembly of humerus mounting block (1), stepper motor mounts (2), worm gear boxes (3), spool rods for spooling fishing line (4), and spool clips (5).....	61
Figure 48: Final design for humerus motor mount housing one Planetary Gearbox Nema 17 stepper motor.....	62
Figure 49: Complete design of assembly for free-standing motor mounting system.....	62
Figure 50: X-ray view of the top (left) and bottom (right) pieces of the humerus.....	65
Figure 51: 3D printed inferior (top) end of humerus.....	66

Figure 52: Full assembly of 3D printed humerus.....	66
Figure 53: 3D print of scapula.....	67
Figure 54: Assembled clavicle, ball joint linkage, attachment block, and heat press inserts.....	68
Figure 55: Final 3D printed version of Rib 5.....	68
Figure 56: Table of rib connection points with its corresponding digital plot (left) that was transferred to the plywood (right) for accurate bone positioning.....	70
Figure 57: Back of the assembly showing bolts from the rib connections, t-slot beam supports, and plywood.....	71
Figure 58: Right-side view of rib assembly.....	72
Figure 59: Anterior view diagram of ligaments and joint capsules that support the shoulder complex.....	74
Figure 60: Side, top, and front view of shoulder model.....	74
Figure 61: Force diagram used to calculate the moment of the humerus at 90 degrees abduction.....	76
Figure 62: Serratus anterior motor mount (yellow) and lower trapezius (gray) shown with motors and fishing line spools installed.....	79
Figure 63: Upper trapezius motor and mount shown from the front side of the board (left) and the back side of the board (right).....	80
Figure 64: Several views of fully assembled humerus motor mounting system.....	81
Figure 65: Fully assembled shoulder model.....	82
Figure 66: Motor Circuit Schematic.....	83
Figure 67: Fully assembled physical circuit.....	83
Figure 68: Example of photo tracking dots used in testing.....	85
Figure 69: Resulting maximum angular displacement achieved by the humerus during abduction.....	88
Figure 70: Relationship between the angle of the scapula and the angle of the humerus during abduction.....	89
Figure 71: Image showing humerus' deviation from the desired plane.....	91

Introduction

The shoulder is considered one of the most complex joints in the human body, having a complex range of motion and an intricate relationship between primary bone structures. This complexity leads to increased vulnerability, making it one of the most injured body parts.

The American Academy of Orthopedic Surgeons reports that four million U.S. citizens experience shoulder pain or injury annually (*How Many U.S. Citizens Suffer Shoulder Problems?*, n.d.). Common shoulder injuries include rotator cuff tears, torn ligaments, shoulder dislocations, broken clavicles, and shoulder instability.

Existing models of the human shoulder have notable limitations that prevent them from accurately replicating shoulder function. Educational models are often seen simplifying complex tissue arrangements and restricting vital bone motion. On the other hand, models used in testing such as crash test dummies typically ignore the complexities of internal shoulder mechanisms and lack accurate material properties. Discovering that there is a lack of physical models that accurately replicate the complex movement of the shoulder was the motivation behind this project. The creation of a physical shoulder model with biomechanically accurate functionality would be extremely beneficial for a variety of applications. Such applications may include the development and testing of injury prevention devices, physical therapy methods, and educational purposes. A model that accurately replicates the human shoulder could provide quantitative measurements surrounding these devices' effectiveness in impact scenarios. Our goal was to create a full-scale automated musculoskeletal model of the shoulder that replicates coronal abduction, in addition to the relative motion of the scapula, clavicle, and humerus. The long-term goal is that our model will be the basis of a more comprehensive rig that can be used in a learning environment for medical professionals, students, or patients. We also believe that this rig could be used in impact testing and the development of protective devices for the shoulder.

Literature Review

Anatomy and Kinematics

General Overview of Anatomy

The shoulder is made up of three bones: the scapula, clavicle, and humerus. Two primary joints in the shoulder that contribute to motion are the acromioclavicular joint and the glenohumeral joint. The acromioclavicular joint connects the acromion, a part of the scapula, and the clavicle (*Shoulder Anatomy, n.d.*). Numerous ligaments comprise the joint capsules connecting the acromion to the clavicle. The glenohumeral joint is where the ball shaped portion of the top of the humerus (humeral head) fits into a shallow cuplike socket (glenoid) in the scapula, allowing a wide range of movement. The surface of the bones where the ball and socket meet are covered with elastic cartilage that absorbs shock and its smooth surface allows the joint to move easily (*Shoulder Anatomy, n.d.*). The labrum is a fibrous ring of cartilage that surrounds the glenoid, to create a deep socket to statically stabilize the humeral head while also providing cushioning that reduces the shock transferred between the humerus and scapula. The rotator cuff connects the humerus to the scapula and is made up of the tendons of four muscles, the supraspinatus, infraspinatus, teres minor, and the subscapularis. Tendons attach muscle to bone. The biceps tendon attaches to the biceps muscle allowing the forearm to rotate. Muscles in turn move bones by pulling on tendons. The muscles of the rotator cuff keep the humerus tightly in the socket. The deltoid lies directly on top of the glenohumeral joint and is the largest and strongest muscle of the shoulder. It provides the strength necessary to lift the arm (*Shoulder Anatomy, n.d.*). General shoulder anatomy is shown below in Figure 1. For additional explanation of medical terminology see Appendix A.

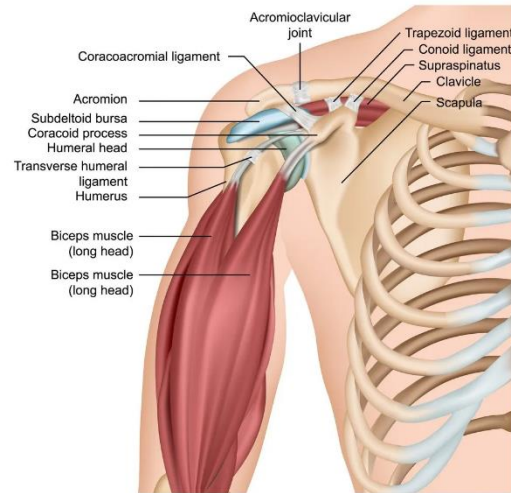


Figure 1: Image of the human shoulder (Source: Shoulder Anatomy, n.d.)

Bones

There are three bones that make up the shoulder: the scapula, the clavicle, and the humerus shown in Figure 2. The scapula is a large, flat, and somewhat triangular bone that sits between the humerus (upper arm bone) and the clavicle (collar bone). The scapula is responsible for stabilizing the upper arm bone, which sits in a shallow socket on the outer edge of the shoulder girdle shown in Figure 3. The scapula has three borders: superior, medial, and lateral. The superior border is the shortest, making up the outer tip of the shoulder. Lying next to the spine is the medial border, and the lateral border of the scapula is located near the armpit. The top of the shoulder girdle and the most superior point of the scapula is the acromion process (*Shoulder Anatomy, n.d.*).

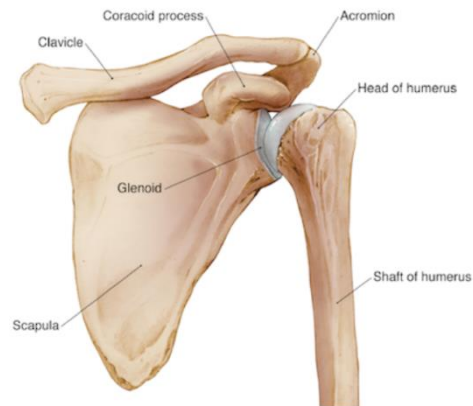


Figure 2: Posterior view of the bones of the shoulder girdle (Source: Shoulder Anatomy, n.d.)

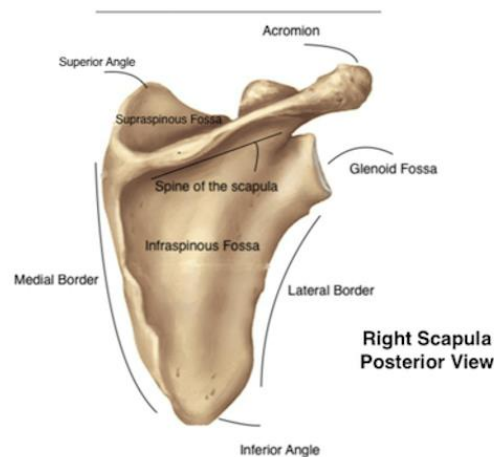


Figure 3: Posterior view drawing of the scapula (Source: Shoulder Anatomy, n.d.)

The coracoid process is the most anterior portion of the lateral border and is an attachment point for many ligaments and muscles. The clavicle is a long, S-shaped bone located between the shoulder and the top of the ribcage. It articulates with the acromion process of the scapula and one end of the sternum. The humerus articulates with the scapula at the glenoid cavity, connecting the body to the axial body. The top of the humerus is rounded and fits into the shallow socket of the scapula, creating the shoulder's ball and socket joint. This construction allows for the arm's large range of motion. (*Shoulder Anatomy*, n.d.)

Musculature

The shoulder muscles have a wide range of functions and play a critical role in providing stability for the shoulder joint. Muscles from the arm, back, chest, and the shoulder itself work together to move the arm. These muscles can be broken into two groups, the anterior and posterior muscle groups.

The anterior muscle group is composed of the coracobrachialis, deltoid, subscapularis, subclavius, serratus anterior, pectoralis major, and pectoralis minor as shown in Figure 4. The coracobrachialis is a long and slender muscle which originates on the coracoid process of the scapula and inserts on the midshaft of the humerus, flexing and adducting the arm. The deltoid muscle has three origins: the body of the clavicle, the spine of the scapula, and the acromion. It inserts on the deltoid tuberosity of the humerus. (*Shoulder Anatomy*, n.d.) The deltoid muscle plays a large role in the abduction of the humerus, which occurs when all its fibers contract simultaneously. The subscapularis originates on the scapula and inserts on the humerus. When this muscle contracts, it will internally and medially rotate the humerus. In certain positions, the subscapularis has some adduction and extension functions. The subclavius is located between the clavicle and the first rib. It works to depress and stabilize the lateral clavicle while the shoulder moves the arm. The serratus anterior is a fan-shaped muscle that originates on the lower ribs and inserts at the entirety of the anterior surface of the scapula. The muscle pulls the scapula forward, which allows for anteversion and protraction of the arm. The pectoralis major is the largest muscle on the anterior chest wall which originates on the clavicle, sternum, and top ribs, and inserts on the sulcus and humerus. The pectoralis major works to rotate and adduct the arm. The pectoralis minor is a small muscle in the anterior chest wall that is attached from the ribs to the coracoid process of the scapula. The pectoralis minor assists with the stabilization of the shoulder complex, protraction of the shoulder, and plays a small role in elevating the ribs. (*Shoulder Anatomy*, n.d.)

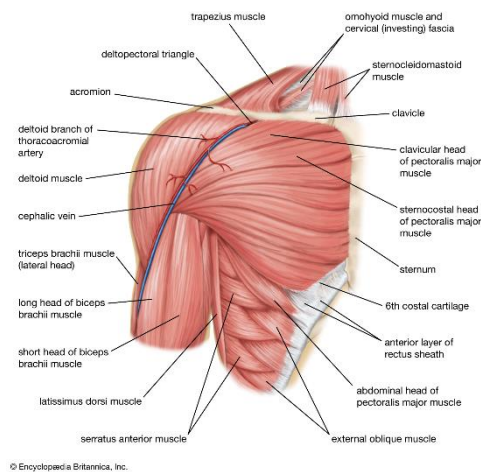


Figure 4: Anterior grouping of the shoulder girdle (Source: Muscles of Shoulder Region | Bone and Spine, n.d.)

The posterior group of muscles is composed of the trapezius, levator scapulae, rhomboids, and the latissimus dorsi, as well as the muscles of the rotator cuff, including the supraspinatus, infraspinatus, teres minor, and teres major, see in Figure 5 below. The trapezius is a broad, flat, superficial muscle extending from the cervical to the thoracic region on the posterior aspect of the neck and trunk. The trapezius contributes to the extension and side flexion of the axial skeleton. It is used to tilt and turn the head and neck, shrug, steady the shoulders, and twist the arms. The levitator scapulae is a thick, strap-like muscle that originates on the upper vertebrae and inserts on the scapula, elevating and abducting it. The rhomboids are a collective group of muscles formed by the rhomboid major and minor. Functionally, the rhomboid muscles retract, elevate, and stabilize the shoulder through articulation with the trunk. The latissimus dorsi is a broad, flat muscle that occupies most of the lower posterior thorax. The primary function of this muscle is to extend and rotate the arm at the shoulder. The final four muscles, the supraspinatus, infraspinatus, teres minor, and teres major, compose the rotator cuff of the shoulder. The supraspinatus originates on the scapula and inserts on the humerus. The supraspinatus muscle is responsible for contributing to multiple functions within the shoulder: abduction of the humerus and stabilizing the glenohumeral joint. The infraspinatus muscle functions by externally rotating the humerus. The teres minor originates at the lateral border of the scapula and inserts on the greater tubercle of the humerus. The teres minor acts to externally rotate the humerus and assist

with abduction of the humerus. (Crim, 2018) The teres major spans from the inferior aspect of the scapula to the proximal end of the humerus. Unlike the teres minor, the teres major does not attach to the glenohumeral joint. The main function of the teres major is to produce movements of the arm on the shoulder joint, and it also contributes to the stabilization of the shoulder joint.

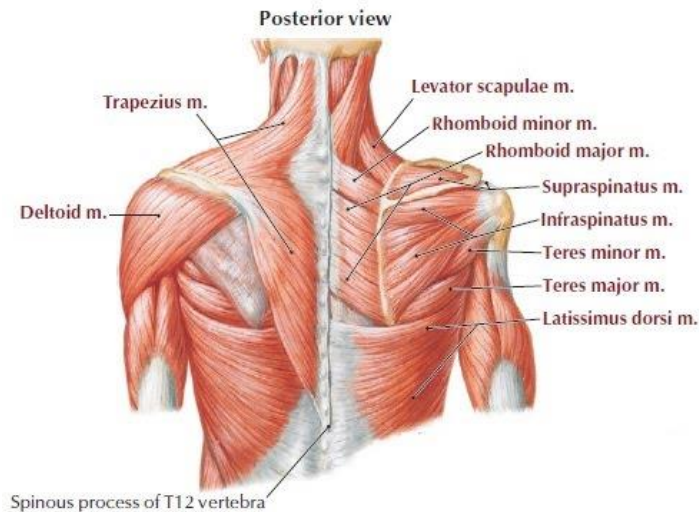


Figure 5: Posterior grouping of the shoulder girdle muscles (Source: Anatomy – Musculoskeletal Ultrasonography, n.d.)

Joints and Ligaments

There are four main joints in the shoulder. The glenohumeral joint is structurally a ball-and-socket joint where the head of the humerus articulates with the glenoid fossa of the scapula, and the glenoid labrum, a ring of cartilage, that supports the humerus at the joint. This joint has both static and dynamic stabilizing structures that allow for extreme degrees of motion in multiple planes of the body. (*Anatomy of the Shoulder*, 2019) The acromioclavicular joint is formed by the lateral end of the clavicle and articulates with the acromion process on the scapula. The acromioclavicular joint is responsible for transmitting forces through the upper limb and shoulder to the axial skeleton. The acromioclavicular joint has limited mobility due to its supporting ligaments, the acromioclavicular ligament, and the coracoclavicular ligament, keeping the shoulder sturdy. The sternoclavicular joint is the only joint in the shoulder that connects the upper extremity to the axial skeleton. This joint works to move the upper limbs. The last joint in the shoulder is the scapulothoracic joint, where the scapula articulates with the

ribcage (*Bones & Joints of the Shoulder* | *ShoulderDoc*, n.d.).

Biomechanics of the Shoulder

The complex movement of the shoulder is attributed to the four joints that comprise the shoulder complex. There are three main degrees of freedom that account for the core movements of the shoulder: flexion and extension, abduction and adduction, and medial and lateral rotation, as shown in Figure 6 below.

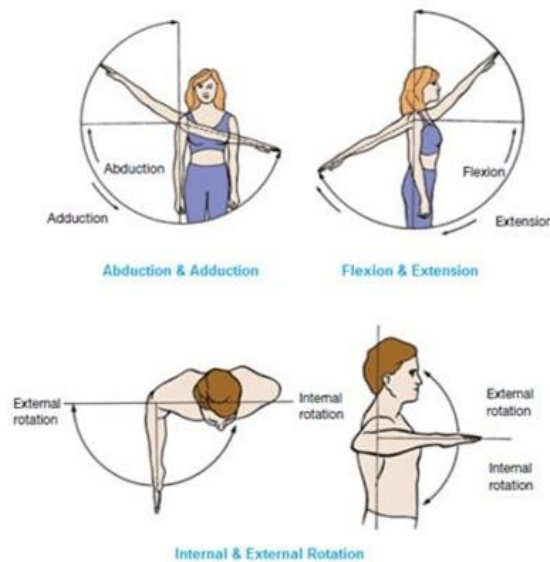


Figure 6: Core movements of the shoulder (Source: “Range-of-Motion-Exercises-for-Shoulder,” n.d.)

Flexion and extension are movements that occur in the sagittal plane and involve anterior and posterior movements of the body or limb. In the limbs, flexion decreases the angle between the bones (bending of the joint), while extension increases the angle and straightens the joint. Abduction and adduction are used to describe the movements towards or away from the midline of the body. Abduction is the movement away from the midline, raising the arm out to the side of the body and adduction is the movement towards the midline. Medial and lateral rotation describe the movements of the limbs around their long axis. Medial rotation is a rotational movement towards the midline, it is also referred to as internal rotation. Lateral rotation is a

rotating movement away from the midline (*Biomechanics of the Shoulder and Elbow | Elsevier Enhanced Reader*, n.d.).

Common Shoulder Injuries

To identify common shoulder injuries, a variety of shoulder injury related studies were researched. Some of the resources from which common injuries were identified were a cohort study at a trauma center in Europe, an ER survey in Norway, multi-year injury observations for a rugby and soccer team, and a review injury history of players participating in the 2004 NFL Combine (Brophy et al., 2007; Enger et al., 2019; Marom & Williams III, 2018; Saw et al., 2017; Stirma et al., 2020). Upon review of these studies, it was concluded that acromioclavicular separation, anterior/posterior instability, clavicle fracture, rotator cuff injuries, and SLAP tears were some of the most common shoulder injuries.

Descriptions of Common Injuries

Acromioclavicular Separation

Acromioclavicular (AC) separation has been reported as the most prevalent kind of shoulder injury in contact sports (Bishop & Kaeding, 2006). According to a study on elite male soccer players from over 50 teams over a ten-year period, AC joint separations and sprains made up 18% of upper extremity injuries (Ekstrand et al., 2012). AC separation occurs when the joint connecting the clavicle to the scapula separates. It is most often caused by an impact directly on the ‘point’ of the shoulder, by falling on outstretched hands or other means of contact. An article from the National Center for Biotechnology Information defines the components of the acromioclavicular joint:

The joint is primarily stabilized by the acromioclavicular ligament, which is composed of an anterior, posterior, inferior, and superior components. Of note, the superior portion of the AC ligament is the most important component for the stability of the AC joint. Supporting structures include two coracoclavicular ligaments (trapezoid and conoid ligaments), which provide vertical stability, as well as the coracoacromial ligament (Kiel & Kaiser, 2021). Figure 7 below shows the components of the acromioclavicular joint.

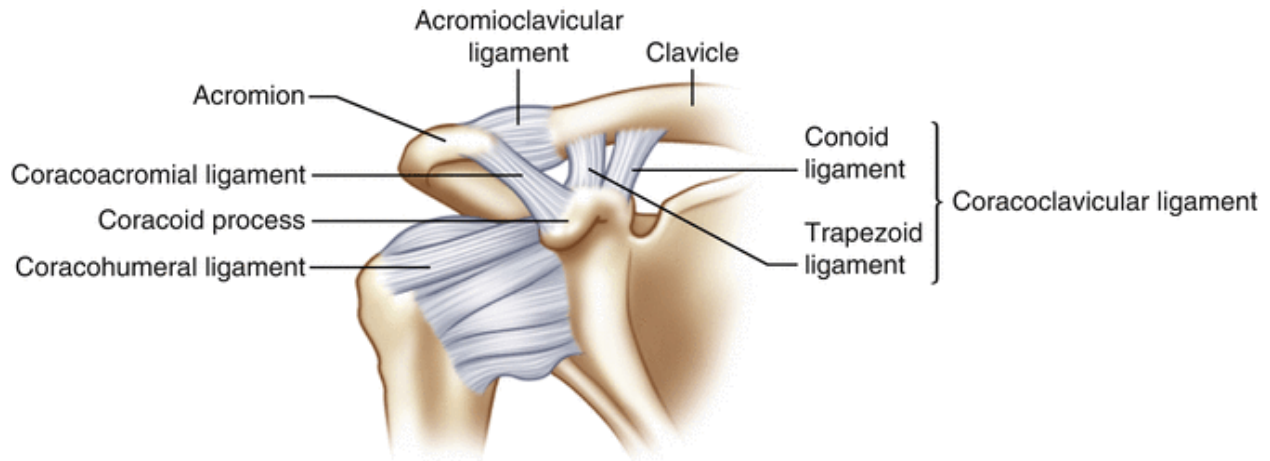


Figure 7: Image depicting AC joint anatomy (Source: *Musculoskeletal Key*, 2016)

Injuries to the AC joint are classified in severity from one to six, with six being the most severe by means of the Rockwood classification system as shown in Figure 8. Classification level is determined by the extent of spraining or tearing that occurs in the various components involved in acromioclavicular separation, including the AC ligament, AC joint, coracoclavicular ligaments, deltoid muscles, and trapezius muscles (Gorbaty et al., 2017).

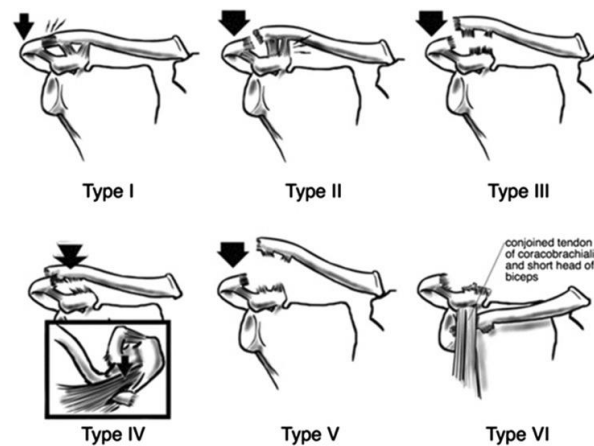


Figure 8: Image of Rockwood Classification of AC Joint Separations (Source: Gorbaty et al, 2017)

Anterior and Posterior Instability

Anterior and posterior shoulder instability, commonly known as shoulder dislocation, occurs when one end of the shoulder joint experiences laxity and the other end is completely dislocated. The shoulder joint is the most frequently dislocated joint of the body (*Dislocated Shoulder -*

Symptoms and Causes, n.d.). Dislocation is commonly caused by a sudden blow to the shoulder or extreme rotation. During dislocation, the humeral head dislocates or sublates from the glenoid fossa, as shown in Figure 9 below. Instability is frequently caused by repeated trauma to the shoulder or a single high-energy trauma event, both commonly found to occur during contact sports such as football and wrestling. Posterior instability is defined as posterior glenohumeral translation, while anterior instability is defined as anterior glenohumeral translation, when that translation occurs outside the normal physiologic translation of the humeral head (Varacallo et al., 2021).

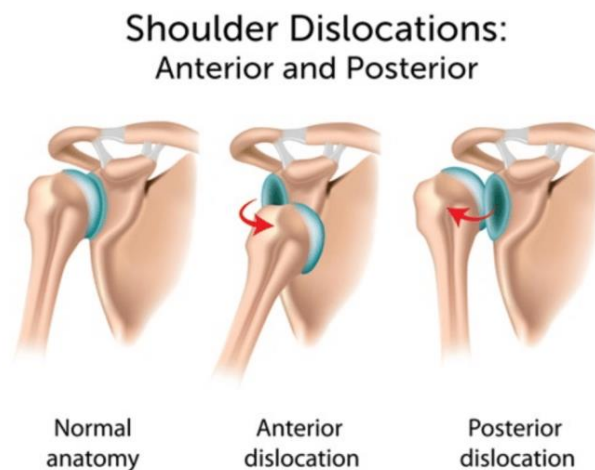


Figure 9: Image of anterior and posterior dislocation of the shoulder (Source: Orthopedic Center for Sports Medicine, n.d.)

SLAP Tears

The term SLAP stands for Superior Labrum Anterior and Posterior. A SLAP injury is defined as an injury to the top part of the labrum, which is a ring of strong, fibrous tissue that helps deepen the glenoid socket and stabilize the shoulder joint. A SLAP tear occurs at both the back and front of the point where the labrum attaches to the bicep tendon at the top of the labrum. This injury is commonly caused by falling onto an outstretched arm, forceful pulling on the arm, forceful movement of the arm when it is above shoulder height, or shoulder dislocation. Repetitive overhead sports may also cause SLAP tears from repeated shoulder motion (*SLAP Tears - OrthoInfo - AAOS*, n.d.). An image showing a SLAP tear is shown below in Figure 10.

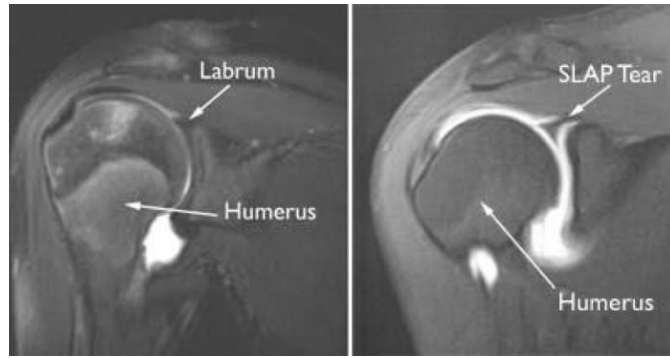


Figure 10: MRI image of healthy shoulder (Source: American Academy of Orthopedic Surgeons, 2019)

Clavicle Fracture

Clavicle fractures are caused by impact trauma, commonly incurred through sports injuries or falls. Most clavicle fractures do not require surgery, but more severe breaks may require surgery to realign the bone and implant structural supports to hold the bone in place while it heals

(Broken Collarbone - Symptoms and Causes, n.d.). A fractured collar bone is shown in Figure 11.

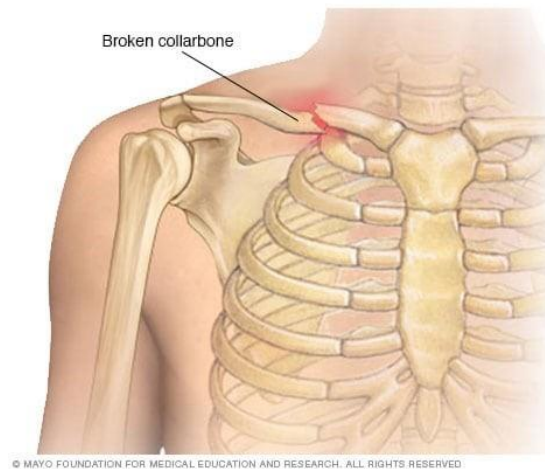


Figure 11: Image depicting a broken collarbone (Source: Mayo Clinic, 2011)

Rotator Cuff Injury

The rotator cuff consists of several muscles and tendons working in tandem to surround and support the shoulder joint. Included muscles are the subscapularis, the supraspinatus, the infraspinatus, and the teres minor muscles. These muscles all end in fibrous tendons of the same

name of the muscle they are attached to There is also a lubricating sac called a bursa that sits between the rotator cuff and bone on top of the shoulder which may become inflamed when a rotator cuff injury occurs. A rotator cuff injury is typically defined as a tear of any of the involved tendons within the rotator cuff, as shown in Figure 12. The rotator cuff can be damaged through substantial impact to the shoulder or wear and tear (Brand, 2008).

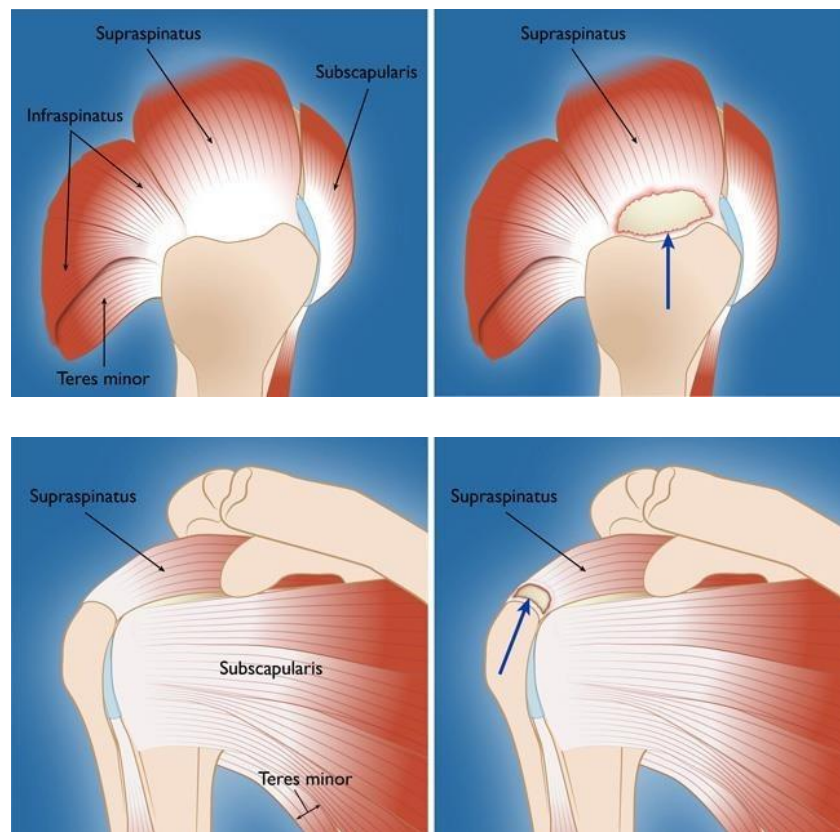


Figure 12: Image of healthy rotator cuff anatomy (Source: Ortho Info, 2021)

Existing Shoulder Models

Realistic Educational Models

The ability to make accurate anatomical models based on medical imaging has been made possible by new 3D printing technology. Various types of printers can create elements allowing for the reconstruction of full joints equipped with bones, ligaments, and muscles. 3D printed models for educational purposes often don't need to have the anatomical accuracy of more advanced clinical models. They instead rely more on the variety of new materials that can be 3D

printed, many of which can closely replicate these bodily components in both texture and functionality.

Design Software

From doctors to engineers, there are many individuals within the biomedical field that benefit from the production and use of bio-CAD models. Bio-CAD refers to the application of computer aided design to create three dimensional models of various biological elements, typically parts of the human body (Sun et al., 2005). These models can vary in accuracy and functionality depending on their intended use; however, most models follow roughly the same path towards creation. CAD models are commonly used for on-screen visual aids, FEA (finite element analysis), and 3D printing of physical models. There are numerous commercial efforts to refine and simplify the creation of both the bio-CAD model and its 3D printed counterpart to be used in a wide range of applications. Processes and technologies have advanced the field in a way that allows for the creation of bio-compatible components that can be implanted within the human body during numerous medical procedures (3D Printing in the Hospital, n.d.). When focusing specifically on educational models, there are two main uses: the training of medical professionals and data analysis through simulation. Our project will focus primarily on models created for data analysis and testing; however, our background research attempts to provide an overarching view of the field as a whole.

Imaging and Virtual Modeling Techniques

The first step in creating a bio-CAD model is gathering medical data from which to create the basic framework. The most common practice for gathering initial data is through non-invasive imaging techniques such as computed tomography (CT) and magnetic resonance imaging (MRI) (3D Printed Medical Models – State of the Art 2021, 2021a). Optical microscopy is another technique used; however, this process is more complex and requires the use of small-scale imaging making it unideal for re-creating large sections of the human body. Both MRI and CT scans result in an accumulation of 2D images that when “stacked” on top of one another create an outline of the three-dimensional shape you wish to model (Sun et al., 2005). President of BMi Inc., Dr. Crispin Weinberg describes the next step as being the creation of a “point cloud” or a series of points in three-dimensional space that essentially outline the structure to be modeled

(Dr. C. Weinberg, personal communication, September 9, 2021). This type of model typically can be used for 3D printing in the form of an STL file but lacks the structure necessary for FEA testing and/or editing within modeling software. The process of converting this mesh file to an actual 3D model is a complicated one, but there are several leaders in the commercial field that specialize in this work.

Leaders in the Field

Specialists in converting medical image data to 3D models include Dr. Weinberg's BioCAD by BMi Inc. along with SurgiCAD by Integraph ISS, MedLink Imaging by Vieworks, and Mimic/MedCAD by Materialise (Sun et al., 2005). Materialise and BMi each have sectors tailored towards the creation of commercial models for a variety of uses. BioCAD is a service BMi provides that creates specialized CAD models based on imaging data. These files are compatible with the CAD software Solidworks allowing for advanced FEA testing as well as model manipulation. STL files of a shoulder joint comprised of numerous bone and soft tissue structures can cost over \$500. STL files can be used for 3D printing applications but the file itself cannot be edited. The price nearly triples when looking to purchase a manipulatable CAD file with the same elements (Dr. C. Weinberg, personal communication, September 9, 2021). Materialise provides services that transform medical scans into 3D anatomical models and assist the consumer in the printing process. The company's files are compatible with a number of 3D printers, and they even offer a service to help the consumer select the best printer for their given needs (Go from Scan to 3D Model | Materialise Mimics InPrint, n.d.). This company primarily serves hospitals looking to implement 3D printing solutions within their practice. These 3D printed parts can be used in the training of medical professionals as well as bio-compatible implants that are approved for use in surgery. The company does, however, have a sector donated to educational modeling and analysis.

3D Printing Biomedical Models

Stratasys is a pioneer in the field of commercial 3D printing. They serve many well-known companies such as Google, Ford, and countless others with prototyping and design assistance and have also expanded into the medical industry. They produce a J750™ Digital Anatomy™ 3D Printer that specializes specifically in the creation of medical models. Additionally, the company

has a variety of printing materials that are designed to mimic the external texture and internal structure of various soft tissue materials (*Feel the Difference. Stratasys J750™ Digital Anatomy™ 3D Printer.*, n.d.). It is unclear as to how accurately these materials replicate the mechanical properties of actual tissue in terms of strength, elasticity, and more. Another printing company that has directly targeted the medical community is Formlabs. The company has formed a partnership with GE Healthcare's Advantage Workstation to establish a software base that converts medical imaging data into files that are compatible with their printers (3D Printed Medical Models – State of the Art 2021, 2021b). Formlabs uses a style of printing known as resin 3D printing where a liquid material is cured to a build plate using advanced laser technology. Much like Stratasys, they have a printer model (the Form 3B) along with an array of resins that are specifically designed for medical modeling. A slightly lower quality but more cost-effective option employs the use of the Ultimaker. Their model, the Ultimaker S5, is commonly used in combination with Materialise biomedical modeling software discussed previously in the Design Software section (3D Printed Medical Models – State of the Art 2021, 2021b). Both Formlabs and Ultimaker printers are commonplace in many technology spaces and are more readily available to the average consumer than Stratasys products. Numerous other companies excel in the printing of biomedical models; however, we chose to narrow our research to these three to encompass a range of printing quality, ease of use, and cost effectiveness.

Full joints within the human body are incredibly complex mechanical and biological systems. They contain numerous components of various materials all working together to allow for a certain range of motion. Ball and socket joints such as the hip and shoulder have an extensive range of motion that is difficult to replicate in a 3D model. Research shows that no models have been created to date with the intention of being used in a mechanical testing setting. Various manufacturers work to create models that include anatomical accuracy and in some cases movement that seeks to mimic actual joints. Monash University in Australia has an extensive 3D printing laboratory that specializes in biomodelling. They have used CT scan data with Mimaki and Formlabs printers to create an extensive library of models of the entire human body (*Monash 3D Printing - Monash Biomedicine Discovery Institute*, n.d.). Their “Deep Dissection of a Right Shoulder Girdle” model (Figure 13) is a highly accurate, fully 3D printed model of the human shoulder, complete with numerous muscles, tendon, and ligament sections.



Figure 13: Example model of right shoulder girdle created by Monash University (Source: Anatomical Models | Human Joint Models)

3B Scientific and SOMSO are two medical modeling companies that each produce a model shoulder that claims to replicate shoulder motion. Both models specify that motion includes abduction, anteversion, retroversion, as well as internal and external rotation. They do not specify actual angle measurements achieved during rotation which could quantitatively determine whether they correspond with shoulder functionality. Additionally, each contains the classic three bone structure comprised of the humerus, scapula, and clavicle along with various accompanying ligaments and tendons. Neither model includes the complete array of soft tissue sectors within the shoulder, leaving out various ligaments and tendons while disregarding muscle groups all together. It is unclear what materials were used and what method was used to create each model whether it was some form of casting, 3D printing, or other modeling processes. 3B Scientific's "Deluxe Functional Shoulder Joint Model" (Figure 14) includes two tendons and six ligaments as labeled in Figure 15 below (*Anatomical Models | Human Joint Models | Deluxe Functional Shoulder Joint Model*, n.d.).

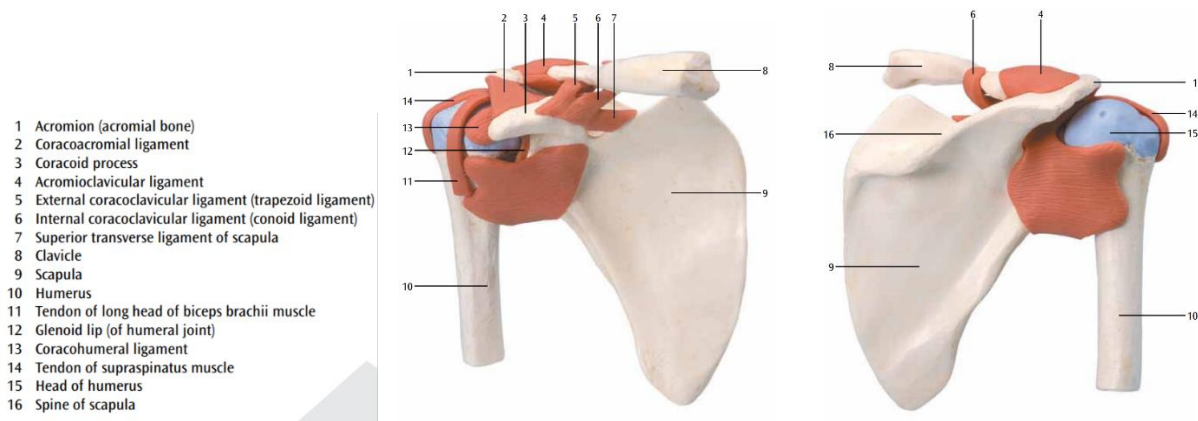


Figure 14: “Deluxe Functional Shoulder Joint Model” by 3B Scientific (Source: 3B Scientific, n.d.)

Similarly, SOMSO’s “Functional Model of the Shoulder Joint” (Figure 15) has six ligaments and one tendon as shown in the figure below. An additional unique feature this model offers is detachable ligaments/tendons allowing for increased visibility of the inner components of the joint (SOMSO *Functional Anatomy Model of the Shoulder Joint*, n.d.).

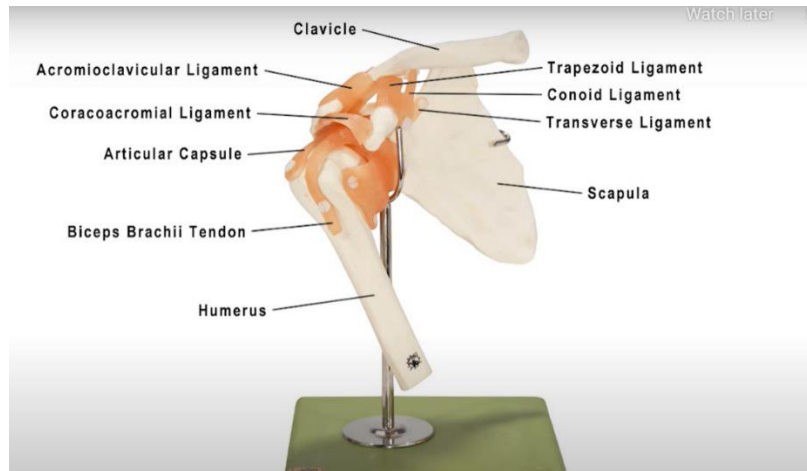


Figure 15: “Functional Model of the Shoulder Joint” created by SOMSO

A model made in 2017 replicated the muscles of the shoulder using linear orthodontic elastics to identify forces on specified parts of the shoulder joint while in different positions. The shoulder model replicates forces exerted by muscles on bones by representing the muscle with an array of linear elastics connecting between the origin and insertion of the muscle on the bone. The

combined force created by the elastic will be equivalent to what the muscle produces. The model was positioned into three different equilibrium positions (60 degrees flexion, 60 degrees abduction, and 30 degrees abduction and flexion) by adjusting the length of the chains representing each muscle. The model is shown below in Figure 16.

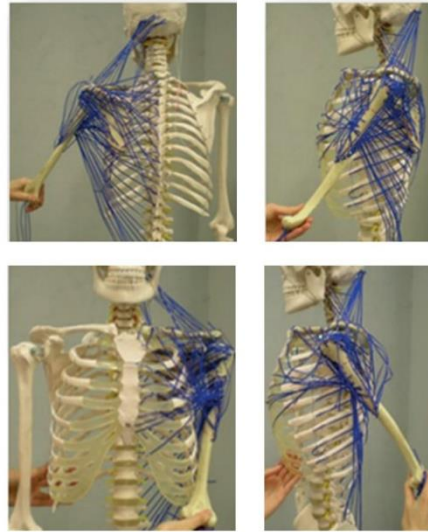


Figure 16: Shoulder model created by Almeida-Galárraga et al. (Source: Almeida-Galárraga et al., 2017)

A series of steps enabled calculation of the forces that would be exerted by each muscle. First, the difference in the number of holes in the chain when the muscle was in a resting position versus when it was in the equilibrium position were counted. From this number, the change in length of the muscle could be calculated. Finally, the force was calculated by multiplying the change in length by the spring constant of the elastic. The model succeeded in displaying relative muscular forces that mirrored those found in the human shoulder. However, the authors did not quantitatively define or discuss the scapulohumeral motion. The model was also limited by the use of non-actuated elastics as muscles, as there was no opportunity to display continuous movement of the shoulder.

FEA Models

The shoulder has been a long-studied joint in the human body with an impressive range of motion and stability; however, the internal loading and forces on individual components have yet to be fully understood (Zheng et al., 2017). The shoulder is one of the most difficult models to

reproduce and some biomechanical models provide insight into the mechanics of musculoskeletal function. Unfortunately, these models are often limited in scope due to the complexity of materials and physics occurring within the joints (Bednarski et al., 2019). The finite element method (FEA) has become increasingly popular to assess and predict forces, stresses, and strains transmitted through tendons, muscles, and other elements of the body (Behrmann et al., 2012). Computer software like Ansys, COMSOL, or Abaqus analyzes a model and divides it into a finite number of small nodes in a mesh, creating the finite element. The program then runs equations on these small elements, compiles and interpolates all the calculations, and determines the result on the model. Researchers use FEM to analyze systems with complex geometry, nonlinear materials, and extreme conditions to observe effects and forces in the internal components. Many of these internals have previously not been seen due to the ethical issues that arise with testing extreme conditions on human subjects. Some models have become advanced enough to be a tool for preoperative planning with implants while others are able to assess the state of the soft tissues during rehabilitation after injury (Bednarski et al., 2019). Other models are used to further the understanding of the shoulder by researchers, medical professionals, and patients.

Errors in finite element analysis can arise when oversimplification occurs. Muscles are anisotropic, non-homogenous, elastic, fibrous materials that are often too complex to mathematically calculate forces on every single strand. This leads to muscles being grouped into clusters, consequently overestimating muscle forces (Behrmann et al., 2012). Even advanced models present their limitations in the variability of the length in the fibers for the muscles, allowing the scapula to move in an unnatural way (Seth et al., 2019). In addition, models using the finite element method that neglect scapulothoracic motion hinder the understanding of how the shoulder functions, as the scapula plays a necessary role during both injury and movement (Bolsterlee et al., 2013). Swedish Shoulder Model (SSM) uses the shoulder rhythm (Yang et al., 2010) as input for scapular motions which is useful for collecting simplified kinematic data. This limits the model to be used only in applications where scapular motion is not disturbed. By using this shoulder rhythm simplification to mimic the natural movement, the shoulder model cannot exhibit shrugging or independent movement of the scapula and humerus. This simplification causes implausible forces in the rotator cuff muscles and deltoids to manipulate the scapula (Seth

et al., 2019). Although the Delft Shoulder and Elbow Model has been validated through electromyography (EMG) signals, the generic inverse dynamics optimization model underestimates the glenohumeral-joint reaction forces during abduction, forward flexion, and other typical dynamic tasks (Asadi Nikooyan et al., 2011).

Replication and Activation Techniques

To raise an arm, the nervous system sends an action potential, or a signal that travels through motor neuron cells. After traveling through the nervous system, the action potential reaches a neuro muscular junction where a chemical is released by the motor neuron. The chemical binds to and creates a reaction with the outer muscle fiber (Body, n.d.). There are three types of muscle contraction: concentric, eccentric, and isometric. Isometric contraction does not cause motion, whereas during movement of the shoulder there are muscles working in concentric contraction while others are in an eccentric contraction. To achieve flexion of the arm, the biceps brachii requires concentric contraction and the triceps brachii lengthens in an eccentric action (Padulo et al., 2013). Several different techniques have been developed to try to replicate the activation of muscles with mechanical replacements.

Cable-Winch Actuation

Kai-Hung Chang of Carnegie Melon University outlined a design process for a winch-cable design based on biological muscular structure in their master's thesis on Automated design, accessible fabrication, and learning-based control on cable-driven soft robots with complex shapes. A winch system cable and winch are used in combination with a sheath to actuate the system. The winch that is attached to the braided nylon fibers is cranked in towards the DC motor, creating a tension force within the fibers. This configuration is displayed in Figure 17 with an additional sheath around the cable in regions where there should be no deformity.

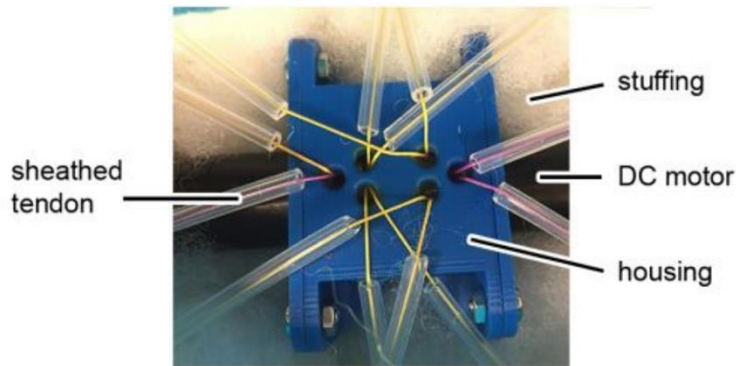


Figure 17: Cable-sheath setup with stiff tube sheath (Chang, 2018)

Pneumatic Artificial Muscles

Pneumatically activated artificial muscles are a popular strategy for dynamic muscle replication. One popular type, known as a McKibben muscle, consists of a pneumatically activated inner tube or bladder inside a braided mesh. An air tube is connected to the inner tube, so that the inner tube may be pressurized. Increasing the pressure in the inner tube causes it to expand, causing the mesh to act like a scissor linkage, turning the radial expansion of the tube into linear contraction of the system as shown below in Figure 18 (*Pneumatic Artificial Muscles*, n.d.).

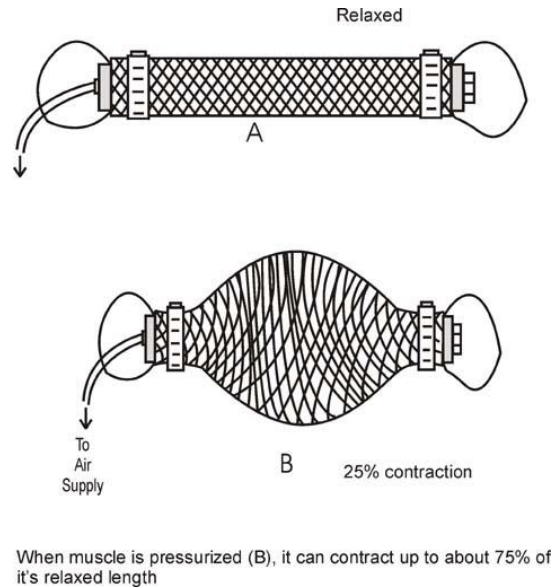


Figure 18: Example of relaxed non-pressurized and activated pressurized McKibben muscle (Pneumatic Artificial Muscles, n.d.)

McKibben muscles are great for replicating muscle for several reasons – they are lightweight, easy to produce, and have load-length curves similar to human muscle. Typical McKibben muscles are capable of about 25% contraction, but altering what materials used can increase that value to as much as 40% (Davis et al., n.d.). Skeletal muscle in humans can generally only contract about 30%, therefore McKibben muscles can achieve realistic muscle contraction lengths. McKibben muscles also produce a contraction force that decreases with their contraction ratio, which is consistent with human muscle behavior.

The inner tube of a McKibben muscle is typically made from an elastomeric material such as silicone. Thinner tubing makes inflation more efficient but contributes to a higher risk of tearing or popping after frequent wear when rubbing against the outer mesh. The braided outer mesh surrounding the tube is typically made from nylon. The initial braiding angle of the mesh is an important factor affecting the maximum force and contraction the muscle can achieve.

A 2016 project used McKibben muscles to build a lower robot that could achieve motions like that of the lower body of a human. The robot consisted of groups of thin McKibben muscles attached to a replicated human skeleton in places where muscles would be activated using air pressure. An image of the robot is shown below in Figure 19 (Kurumaya et al., 2016).

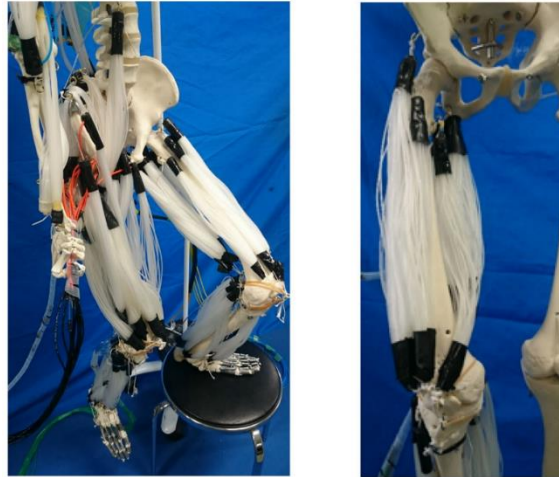


Figure 19: Example project that was built using grouped McKibben muscles (Kurumaya et al., 2016)

Literature Review Conclusion

The prevalence of shoulder injuries generates a need to better understand the forces experienced inside the shoulder. Our research on shoulder anatomy revealed the biomechanical intricacy of its various joints. The complex anatomy and motion make it difficult for researchers to replicate, leading to the rarity of physical shoulder models that accurately replicate its motion. However, several modeling techniques involving Bio-CAD and 3D printing have been used to create shoulder models with varying levels of complexity. Additionally, the development of motor driven, and pneumatic artificial muscles has made it possible to create dynamic models of the shoulder. The accumulation of this research could lead to the development of a revolutionary physical shoulder model that accurately replicates shoulder biomechanics and provides insight into how the human shoulder acts under different conditions.

Methodology

Short-term Project Goals

Design and Construction Goals

1. Manufacture life-size bones involved in scapular humeral motion on the right side of the body: humerus, scapula, clavicle, and all ribs (1-12)
2. Design a base structure to support a fully assembled shoulder mechanism with accurate relative positioning of each bone structure
3. Implement a system of linear attachments representing ligaments in the shoulder
4. Implement a system of linear attachments that can be mechanically driven to replicate muscles during activation

Model Movement and Positioning Goals

1. Accurate anatomical positioning of the primary bone structures (the humerus, scapula, and clavicle) relative to the ribcage and spinal plane
2. Achieve half the total range of motion for humeral abduction or 90 degrees of abduction
3. Replicate the complex relative motion between the scapula and humerus during abduction, commonly known as scapulohumeral rhythm

Long-Term Goals for Future MQPs:

1. Utilize materials that accurately represent the material properties of the tissues in the shoulder to replicate ligaments, tendons and muscle
2. Expand range of motion to include the full range of motion of abduction, adduction, and forward flexion
3. Measure forces being experienced by tissues in the shoulder during various impacts and stresses
3. Develop a testing configuration to replicate common impact scenarios for the shoulder and monitor the forces experienced throughout the shoulder
4. Ease of adaptation by future project teams

Model Movement and Positioning Goals

The three movement and position goals listed above indicate the primary quantitative goals that were most involved in testing. Each of the three goals represents a particular area in which we were able to define anatomical accuracy. They can be summarized as follows: accurate positioning, achieving target range of motion, and replicating relative motion.

Goal One: Accurate Positioning of the Scapula

The section below further explains how we will quantitatively define relative motion between the scapula and the humerus. This motion is commonly known as scapulohumeral rhythm, and it defines the relationship that exists between the movement of the two bones. In order to achieve this relative motion, we must first ensure that the resting position of the scapula is anatomically accurate. The scapula has three degrees of rotation as shown in Figure 20 below. Upward and downward rotation occurs as the scapula rotates away and towards the spine or medial plane. Posterior and anterior tilting is the vertical rotation of the scapula towards the rear and front of the body. And lastly, external and internal rotation is the horizontal rotation of the scapula towards the rear and front of the body. The scapula's neutral or resting position is shown in Figure 21. At this position the scapula is internally rotated 30-45° from coronal plane, anteriorly tipped 10-20° from vertical, and upwardly rotated 10-20° from vertical. All scapula motion as a result of scapulohumeral rhythm begins at this starting position.

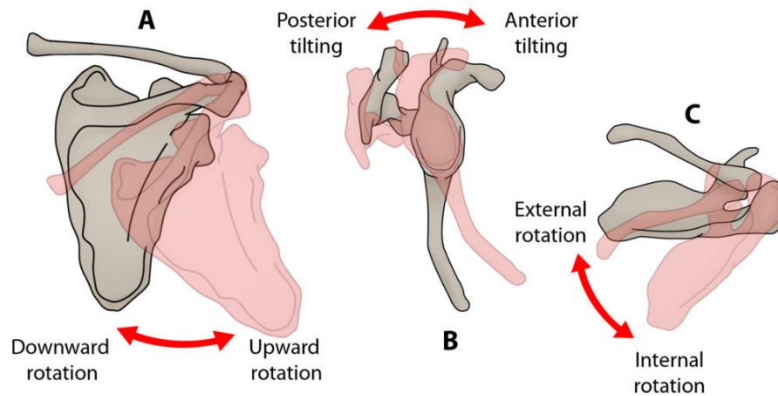


Figure 20: Image of the scapular movements from the back, side, and top view

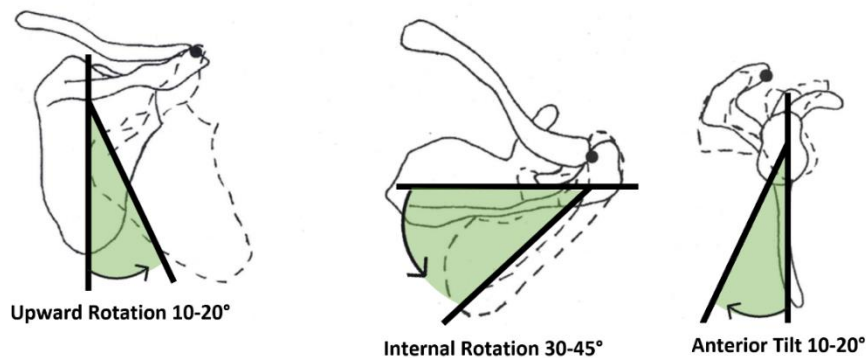


Figure 21: Image of the scapular movements range of motion from the back, side, and top view

Goal Two: Achieve Desired Range of Motion

Scapulohumeral rhythm can be replicated through abduction of the arm. In this body movement, the arm is raised from the side of the body. The arm can raise a total of 180 degrees during abduction, however, for our model we aimed to raise the humerus a total of 90 degrees. To achieve shoulder abduction, there are multiple muscles that work together to raise the arm, these muscles include the supraspinatus, deltoid, trapezius, and serratus anterior. As the arm lowers towards the midline of the body, it is experiencing adduction. This movement relies on muscles including the pectoralis major, latissimus dorsi, teres major, triceps, and coracobrachialis. For the sake of this project, only the muscles involved in shoulder abduction were included in the model. To replicate the motion of adduction, the muscles that were used during abduction were set to move in the opposite direction and were brought to their original position prior to when the arm

was raised when replicating abduction. A more detailed overview of abduction and adduction can be seen below in Figure 22 and 23.

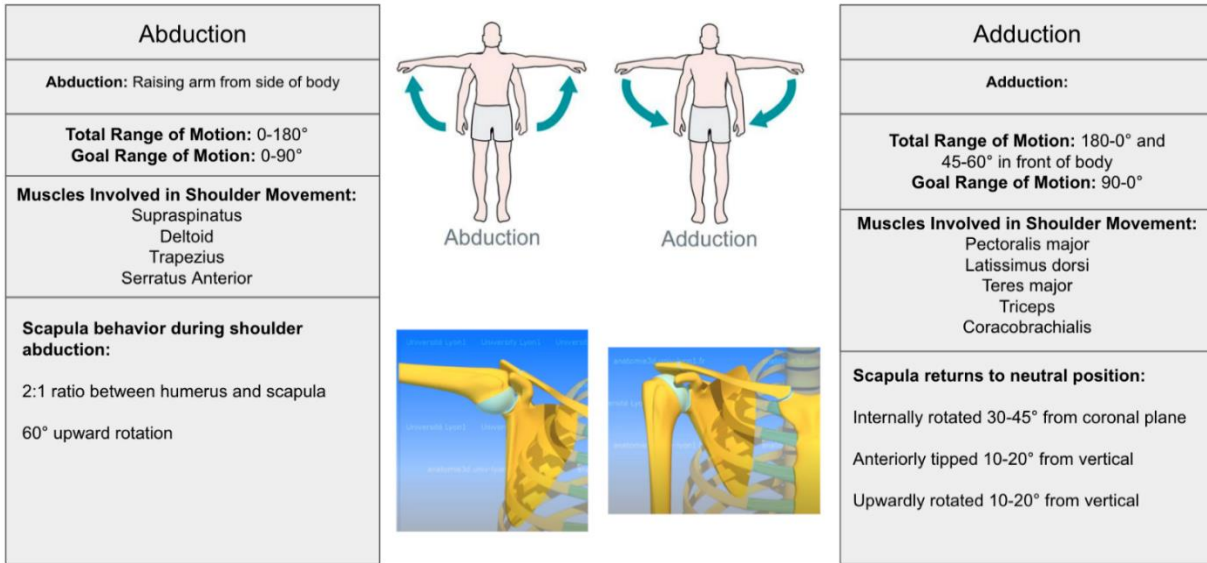


Figure 22: Overview of Abduction and Adduction

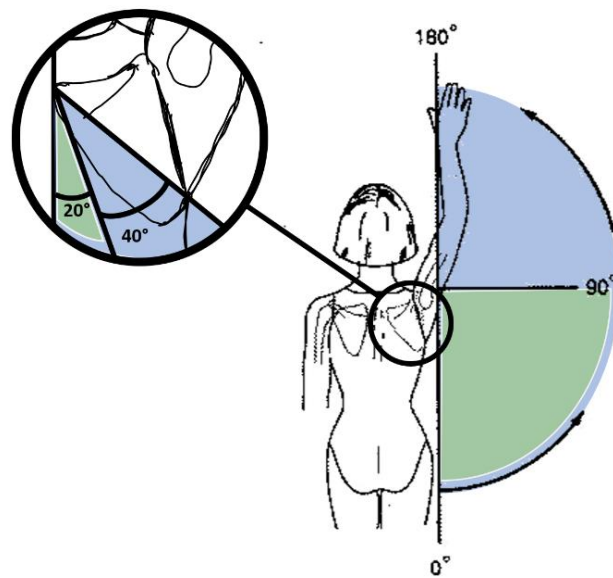


Figure 23: Scapulohumeral rhythm during abduction and adduction

Goal Three: Accurate Relative Motion

The optimal function of the shoulder is reliant on the coordinated movement of the scapula and the humerus. The extensive range of motion that the shoulder can achieve during abduction is much more complex than movement at the glenohumeral joint. Abduction requires coordinated movement between the glenohumeral joint and the scapulothoracic articulation, this is called scapulohumeral rhythm. There are two key motion components of the scapulohumeral rhythm. The first movement is the abduction of the glenohumeral joint, and the second movement is the upward rotation of the scapula. If the scapulohumeral rhythm is properly coordinated, a person would have approximately 120 degrees of glenohumeral abduction and 60 degrees of upward rotation of the scapula. There is about a 2:1 ratio of movement in the glenohumeral joint to that of scapulothoracic articulation. The first 30 degrees of shoulder elevation is referred to as the “setting phase” as shown in Figure 24. As the glenohumeral joint moves past those first 30 degrees of motion, the 2:1 ratio between the glenohumeral joint and the scapula will begin, and the two components will move simultaneously. A visual of scapulohumeral rhythm is depicted below.

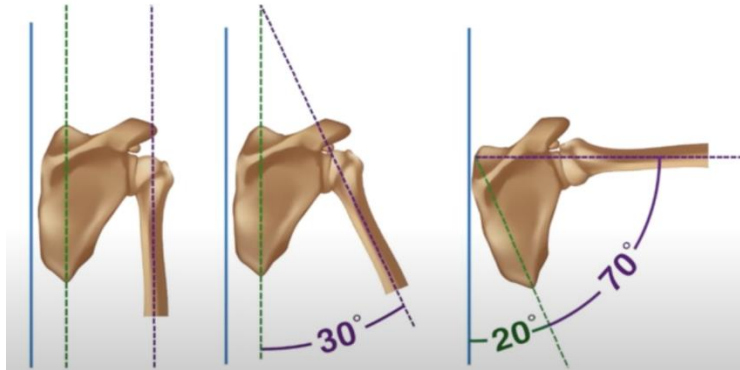


Figure 24: Visual representation of the “setting phase” and the relationship between the glenohumeral joint and scapula during arm movements

Design Concepts: Overall Rig Structure

Throughout the design process, we came up with two main ideas for the mechanical design of our shoulder rig that, in conjunction with soft tissue replication, would help achieve our project goals of achieving specific relative motion of the shoulder.

Design One: Mechanical Scapulothoracic Joint

The design below labeled in Figure 25 shows our initial idea for the shoulder rig. The base structure would include a ground plate and two rods secured perpendicular to it in calculated locations. These rods would serve as connection points to the three 3D printed bone structures of interest: the humerus, the clavicle, and the scapula. The highlight of this design iteration is the slot joint mechanism representing the scapulothoracic joint.

1	Base Plate
2	Primary Rod
3	Secondary Rod
4	Humerus
5	Clavicle
6	Scapula
7	Glenohumeral Joint
8	Sternoclavicular Joint
9	Scapulothoracic Joint

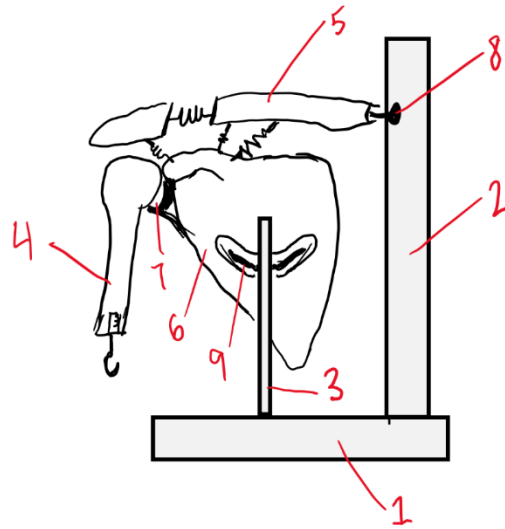


Figure 25: Sketch of design iteration one

Scapulothoracic Joint Design

The attachment of the scapula proved to be the most complex as it moves and rotates, covering six degrees of motion. We designed the mechanism shown in Figure 26 that would be able to achieve our goal range of motion of the scapula. The attachment would consist of a cylindrical rod (the secondary rod) that would be rigidly attached to the base plate at a point directly centered in front of the scapula. Around the rod would be a sliding mechanism that would allow for rotation about the pole along with translation up and down the pole. This would take the shape of a ball bearing with proper lubrication. Attached to this bearing would be a slotted link extruded back towards the scapula, so that it would rest nearly an inch from the bone's surface. The slot would be free to rotate about its connection point with the bearing and from the front view it would resemble a "u". This slot would be concave in the direction of the pole as shown in the top view of Figure 27.

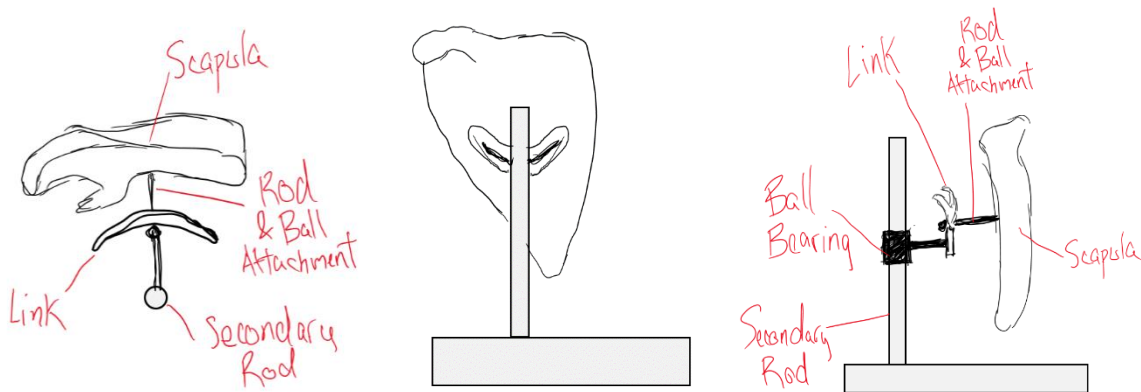


Figure 26: Sketches of top, front, and side view of the scapulothoracic joint

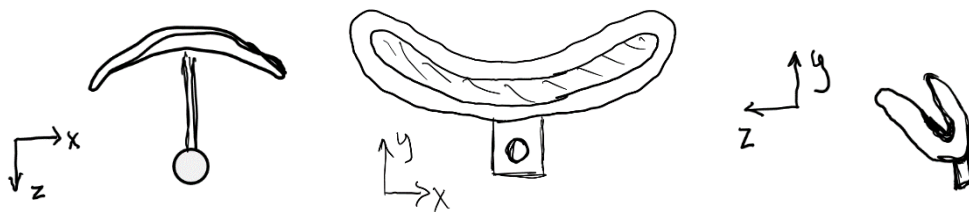


Figure 27: Sketches of top, front, and side view of the unique slot feature representing the scapulothoracic joint

Glenohumeral Joint

Our first iteration of the glenohumeral joint design consisted of a metallic shallow ball and socket joint as shown in Figure 28. In this design, a metallic hemispherical component would be attached to the interior of the humeral head serving as the ball for our ball and socket joint. The corresponding socket on the scapula would be a concave metallic surface in which the ball of the humeral head would rest and rotate within. Since the shallow nature of this interface would make it very unstable, we would implement a magnetic connection between the humeral head and the scapula to act as a joint stabilizer that would mimic the suction forces of the labrum provide in a human shoulder. Ligaments and muscles would further support this joint when they were implemented.

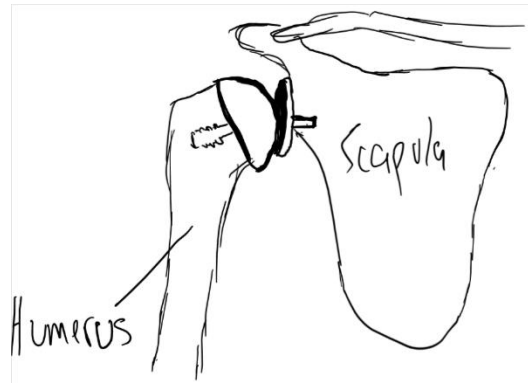


Figure 28: Sketch of glenohumeral joint design

Sternoclavicular Joint

The connection between the clavicle and the sternum was modeled as a ball and socket joint that was created using a metallic ball joint linkage. The end of a human clavicle is capable of rotation at the sternoclavicular joint but has a more limited range of motion than the glenohumeral joint. According to a 2004 study, during the elevation of the arm, “...the clavicle with respect to the thorax generally undergoes elevation (11° - 15° maximum), retraction (15° - 29° maximum), and posterior long-axis rotation (15° - 31° maximum)” (Ludewig et al., 2004). A McMaster-Carr Ball-Joint Linkage has a maximum ball swivel angle of 45° , which is more than enough freedom to cover the range of motion within the sternoclavicular joint (McMaster-Carr, n.d.). For this reason, we chose to use a McMaster-Carr Ball-Joint Linkage as shown in Figure 29 to represent the sternoclavicular joint. The shank end of the ball joint linkage would attach to the rod representing the sternum and the stud end would attach to the end of the clavicle. The overall joint design is shown below in Figure 30.



Figure 29: Sketch of glenohumeral joint design

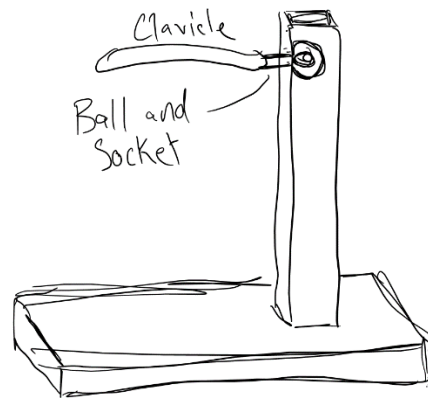


Figure 30: Isolated sketch of sternoclavicular joint design

Design Two: Physical Rib Cage Design

The second design differed from the first in that it included modeling the physical rib cage rather than using a mechanism to take its place, enabling closer replication of the scapulothoracic joint in a human shoulder. Instead of the scapula's range of motion being controlled by the mechanical slot rig shown in design iteration one, the scapula would slide over a model of the rib cage. This in combination with using linear attachments to replicate ligaments, muscles, and tendons would allow us to achieve the relative motion of the scapula, humerus and clavicle as well as their range of motion. Two ideas for the ribcage design are shown below, with Figure 31 showing a solid half-cylindrical sheet being used to model the ribcage, while Figure 32 shows the 3D rendering of a rig where each individual rib is 3D printed to assemble a full ribcage. In the solid ribcage model, the metal sheet bent to represent the ribcage would attach to the two t-slot beams representing the spine and sternum. In the individual ribcage model, each rib would be individually attached to a piece of plywood. The plywood could then be mounted on a t-slot beam base structure allowing for accurate positioning of each rib relative to all other shoulder

components. The glenohumeral and sternoclavicular joints would be the same as that in Design One, except that the shank end of the ball joint linkage of the sternoclavicular joint would now connect to the plywood.

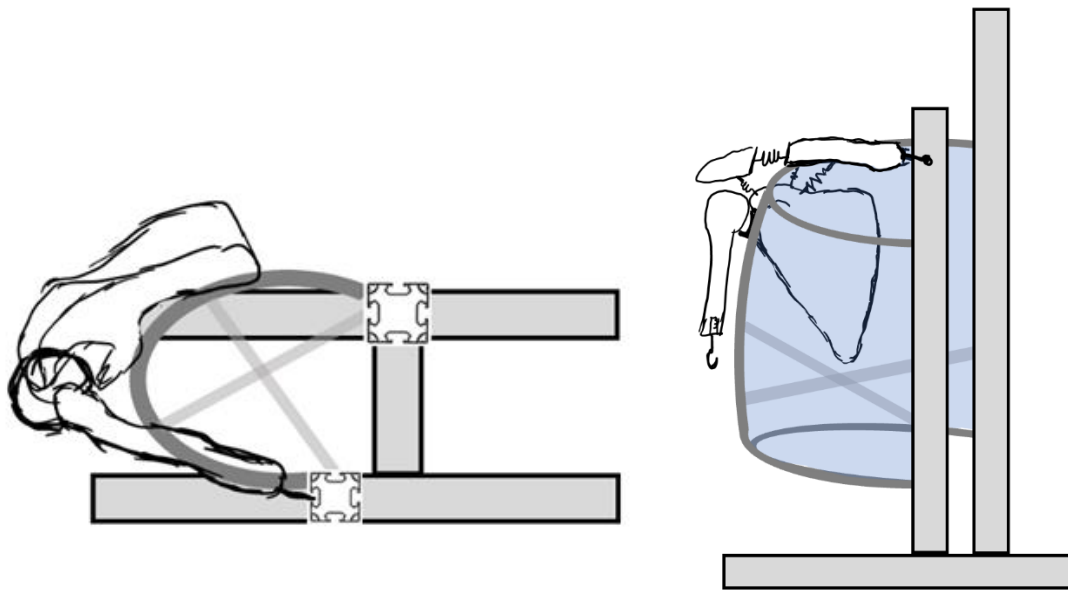


Figure 31: Top view and side view of drawing for a rib cage design concept

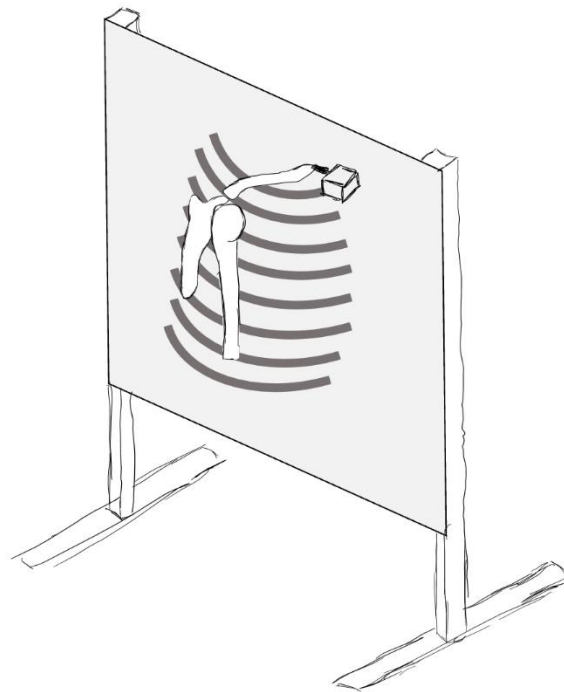


Figure 32: 3D full-scale computer model of rib cage design concept

Final Structural Rig Design

Manipulated Rib Cage Model

For the final design of the structural components of our model, we built upon the individual rib concept from Design Two. To achieve geometric accuracy of the human ribcage in our model, we wanted to obtain a 3D model of the bones of the shoulder that was based off an actual human shoulder. We reached out to Dr. Crispin Weinberg, president of Biomedical Modeling Inc., for assistance as the company specializes in the production of physical and virtual anatomical models based on CT scan and MRI data. We purchased an STL file from Biomedical Modeling Inc. to get accurate models of the three bones of the shoulder (the scapula, humerus, and clavicle) as well as half of a rib cage. This STL file model utilizes the CT scan data from the right torso and shoulder of an adult male, acting as an accurate three-dimensional representation of patient-specific anatomy. The components of the file are shown below in Figure 33 and Figure 34.

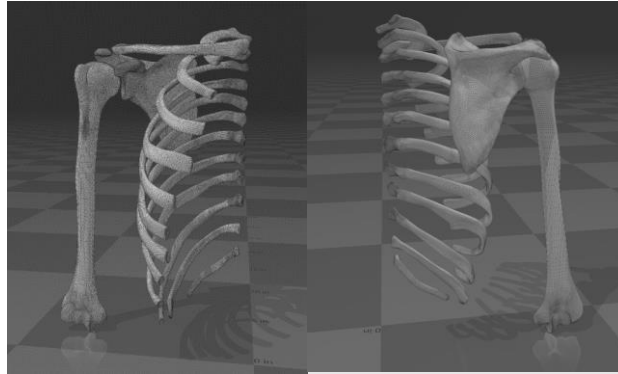


Figure 33: Front and back view of model true to scale (Biomedical Modeling Inc.)

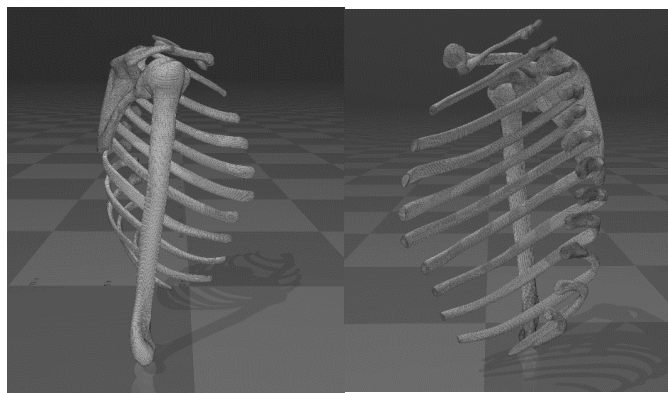


Figure 34: Left and right view of the model true to scale (Biomedical Modeling Inc.)

Building upon this anatomical model, we designed a block connection system that would align all the ribs along the midplane of the body. The CT scan data includes all portions of solid bone but is limited in that it cannot detect cartilage. As a result, the STL structure of each rib is missing a front section that completes the connection to the sternum or midplane. To account for this, a block was added on either end of the rib to complete the full rib as shown in Figure 36. Each block has a width and height of 0.75 in. The resulting 0.75 in x 0.75 in square face was aligned with the end of each corresponding rib. The length was then adjusted to bridge the gap between the end of each rib and a flat plane (modeled in blue in Figure 35) that represents a piece of plywood. The model also shows this “sheet of plywood” secured to a freestanding; t-slot beam structure meant to support the whole model. The full assembly can be seen below in Figure 35, as well as a ribs-only assembly shown in Figure 36.

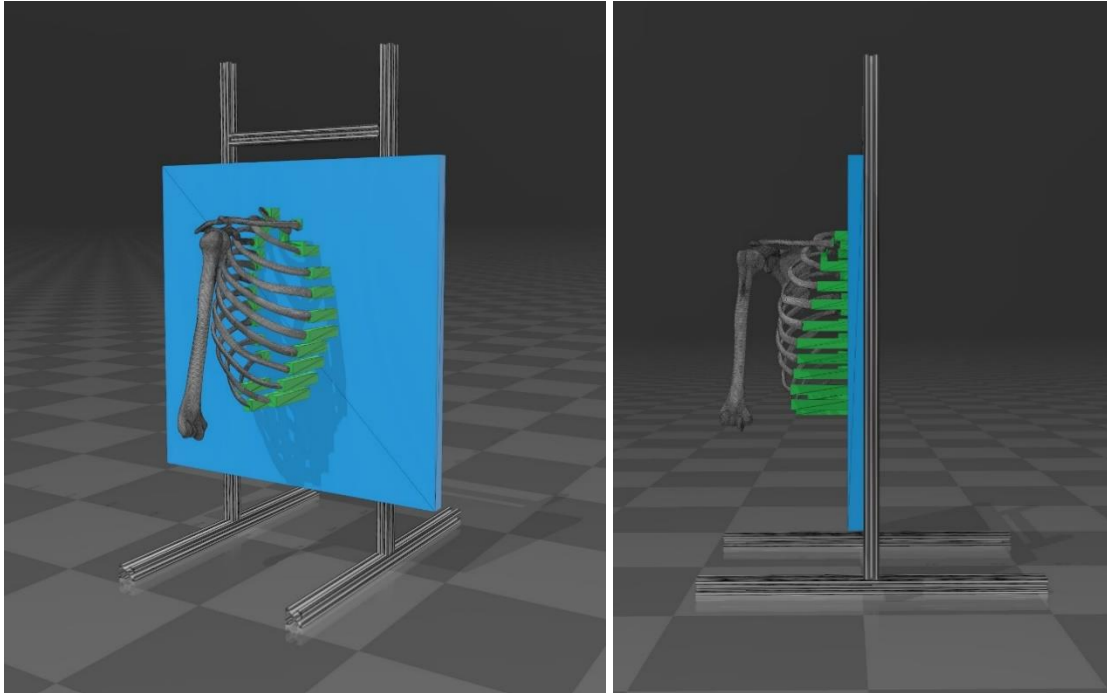


Figure 35: Front and side views of full shoulder rig assembly (without soft tissues)

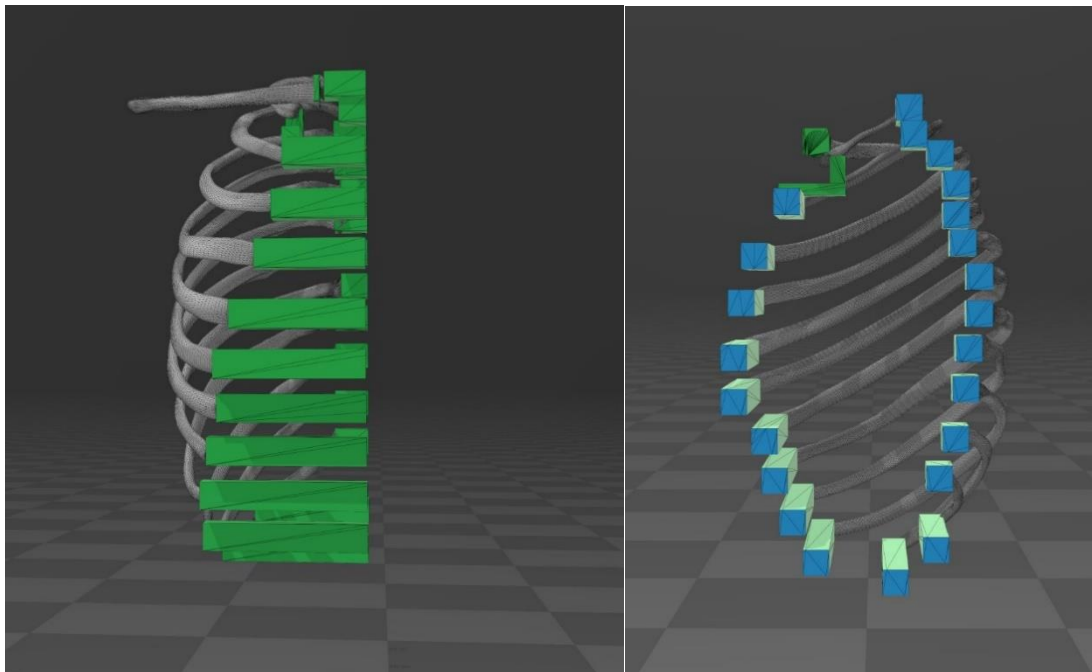


Figure 36: Front and right-side view of rib connections

Sternoclavicular Joint

The end of the clavicle would be attached to the plywood using a McMaster-Carr Ball Joint Linkage as described in Design Two to enable the range of motion of the clavicle provided by the sternoclavicular joint. To achieve proper spacing of the clavicle in relation to the ribs, the location where the clavicle would connect with the sternum would be marked on the plywood, and the geometry of the ball joint linkage would be considered so that the clavicle would be positioned correctly in space. In the design of the clavicle, 1.25" of the end of the clavicle closest to the sternum was removed to provide clearance for the ball joint linkage to connect between the clavicle and the plywood and to provide a flat surface for attachment using a heat press insert. The stud of the ball joint linkage would be threaded into the heat press insert placed in the end of the clavicle, and the shank of the linkage would be threaded into a plywood attachment block mounted to the plywood as shown below in Figures 37 and 38.

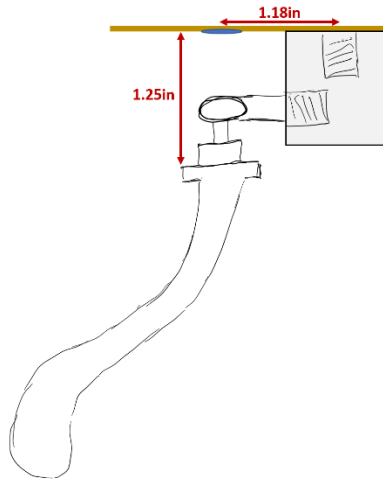


Figure 37: Top view sketch of sternoclavicular joint design

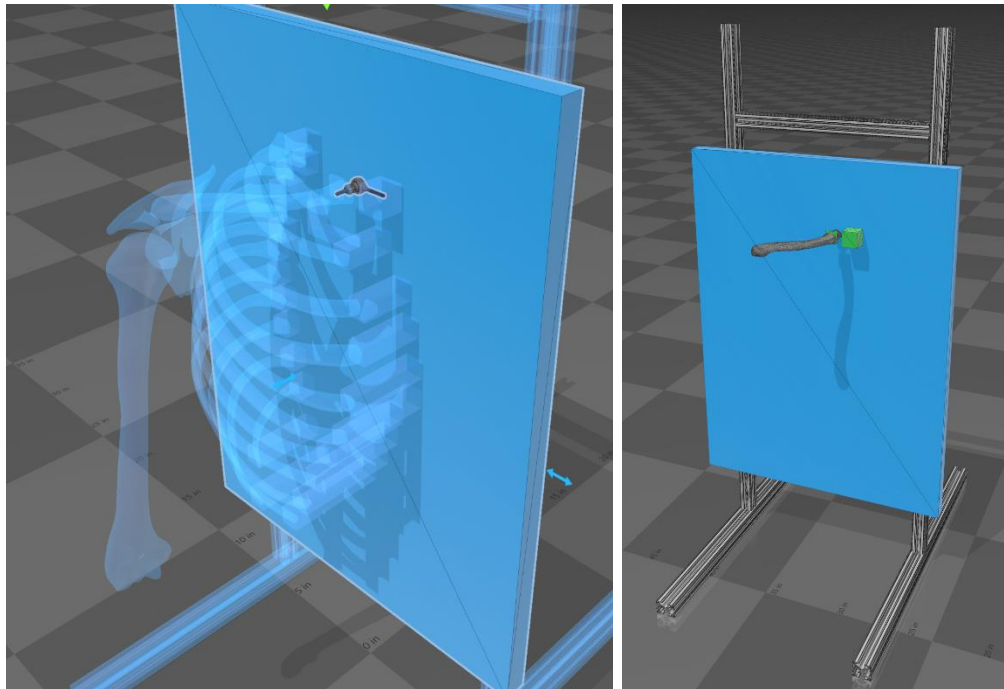


Figure 38: Image on the left is an “x-ray” view of the full shoulder model design and image on the right shows the plywood and support structure with the isolated clavicle

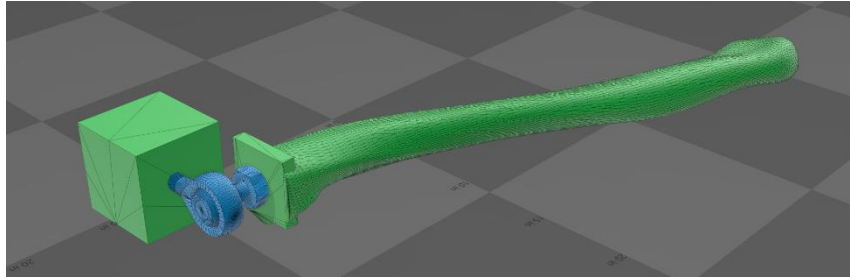


Figure 39: Clavicle and plywood attachments

Glenohumeral Joint

For the final design, we decided to utilize the natural anatomical ball and socket interface created by the humeral head and scapular socket that is present in the STL file model of the humerus and scapula. This was a better option than implementing a ball joint linkage similar to what we had utilized for the sternoclavicular joint due to the extremely wide range rotation of the humerus within the glenohumeral socket. The glenohumeral joint is a synovial joint, meaning it has a flexible fibrous joint capsule surrounding it that allows for an extremely wide range of motion. During flexion, rotation at the glenohumeral joint can contribute up to 100-120 degrees of the overall humeral rotation. When abduction is performed, an average of 43 degrees of rotation has been reported to come from the glenohumeral joint. Since the ball joint linkage has a maximum ball swivel of 45 degrees, using that piece of hardware to represent the joint would limit the range of motion of the joint significantly. To replicate the support provided by the ligaments that comprise the joint capsule that surrounds the glenohumeral joint that stabilizes the humeral head within the glenoid cavity, 3 bungee cords attached to eye hooks inserted into the bones. The bungee cords come with hooks on both ends, allowing the bungee cord securely to attach to the insertion points on the humerus. For the insertion points on the scapula, the hooks attached to the holes drilled near the medial edge of the scapula. The bungee cords ran between, over, and around creating a linear glenohumeral joint capsule that supports the humeral head and allows it to sit in the cavity as shown in Figure 60 further below, while the opposing directions create stability flexibility. while also providing the necessary support during extreme ranges of motion which prevents dislocations.

Soft Tissue System Design

To simplify the complexity of the soft tissues in the human shoulder that contribute to motion and replicate on the kinematics created by the contraction of muscles or support of ligaments, we decided to linearize the soft tissues as much as possible. A computer model shown below showing some of the soft tissue attachments we included in our model is shown below in Figure 40, with linear red lines representing these soft tissues. Although this does not show all the attachments that we modeled and additional muscles we did not include, the linear nature of the soft tissues shown in the figure shows the paths on which we physically modeled our muscles using fishing line in a winch-cable system. For detailed models that label each attachment see Appendix B.

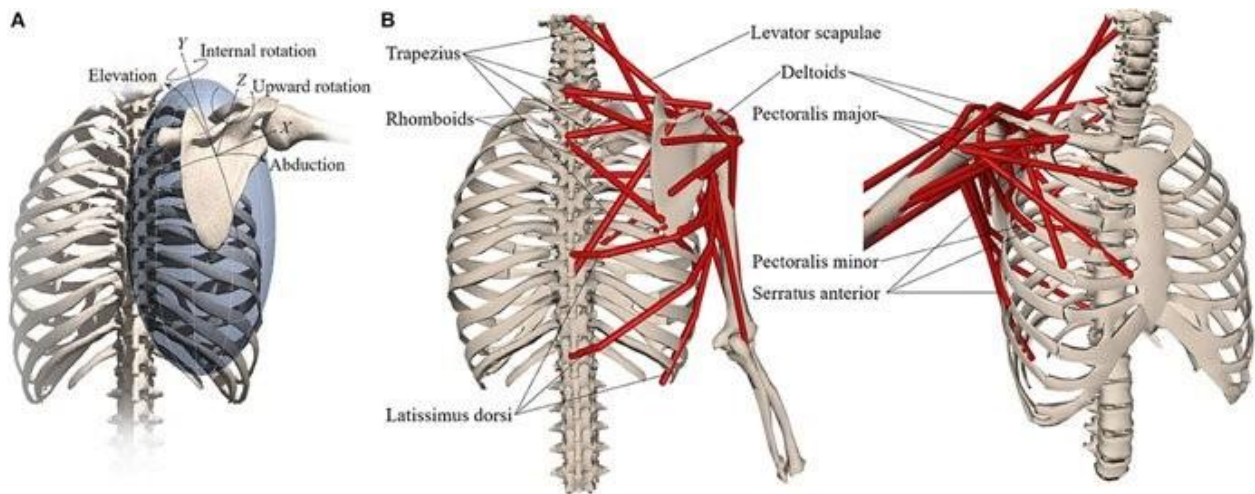


Figure 40: Model from a 2019 study that focuses on kinematically uncoupled movement of the scapula (Seth et al., 2019)

Selection of Soft Tissue Groups

Ligaments

The ligaments shown in Figure 41 below were the glenohumeral ligaments we took into consideration while trying to replicate the glenohumeral joint capsule with multiple bungee cords. The superior (SGHL), middle (MGHL), inferior (IGHL), and spiral glenohumeral ligaments are the main stabilizers of the shoulder that provide the support that keeps the humeral head in the labrum socket in combination with the muscle forces. The coracoclavicular ligaments that connect the clavicle to the acromion of the scapula and the coracohumeral ligaments are also to be included in this model as it creates the connection between the two bones and are linearized

as one linear attachment to simplify our model. The coracoacromial ligament that connects the acromion and conoid process, two locations on the scapula and will also be considered in the replication of the shoulder as it is important to prevent translation of the humeral head.

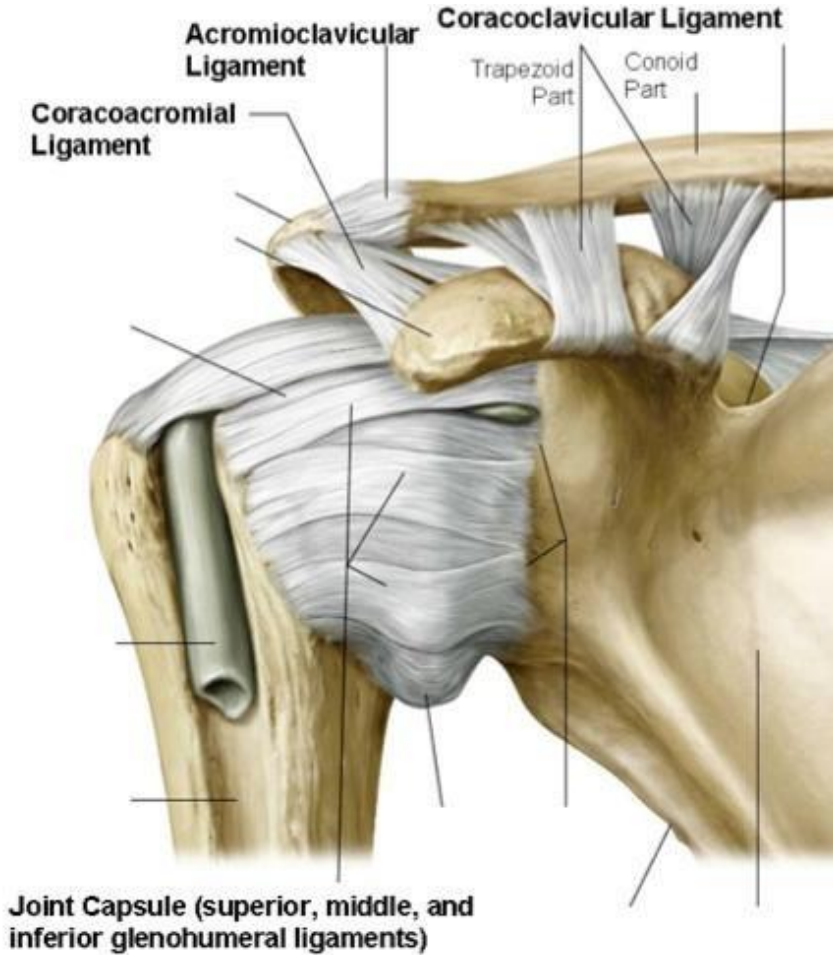


Figure 41: Front view of the glenohumeral ligaments that aid in humerus stability (Shoulder Range of Motion, n.d.)

The acromioclavicular (AC) ligament depicted in Figure 7 earlier in the paper connects the acromion of the scapula to the lateral end of the clavicle. The AC ligament creates a joint capsule that surrounds a cartilage disc. Similar to the function of the labrum, the AC disc provides cushioning in the joint and maintains the lubrication between the two bone surfaces allowing for repetitive movement and force absorption.

5 Muscle Groups

The five muscles we included in our model were the serratus anterior, upper trapezius, lower trapezius, middle deltoid, and supraspinatus. These are the main muscles attributed to humeral abduction in the coronal plane (Lam and Bordoni 2022). While there are other muscles we would wish to include in this model like the middle trapezius, rhomboid major and minor, pectorialis major and minor, teres major and minor, levator scapulae, they are not necessary for abduction of the shoulder and would increase the cost and complexity of our model. Future more robust models would potentially include these additional muscle groups to create additional movements of the shoulder.

Stationary Motor Mounting Systems

Three of the five muscle groups we chose to represent have connections along stationary components in our model such as the ribs or the spinal plane. To provide muscle activation forces along the correct line of action, we determined there would need to be motors aligned along the spinal plane. We chose to secure these motors to the horizontal t-slot beams that connect the two legs of the rig as they are in line with the spinal plane. The beams' locations could be adjusted to better align with attachment locations and t-slot attachments provide an easy way to bolt devices to it.

We used SolidWorks to model a series of motor mounts for two motors options. The mounts are designed to house the motors and are secured to the front face of each motor. They are designed to rest on top of a t-slot beam and connect to either side of the beam using t-slot attachments. Both models are shown in Figures 42 and 43 below.

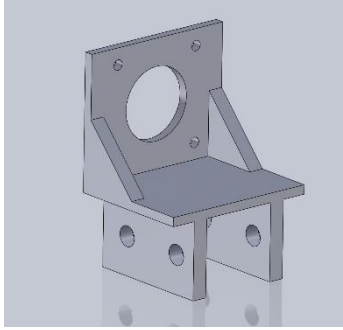


Figure 42: First stationary motor mount designed to secure a single Nema 17 stepper motor to the top of the t-slot beam

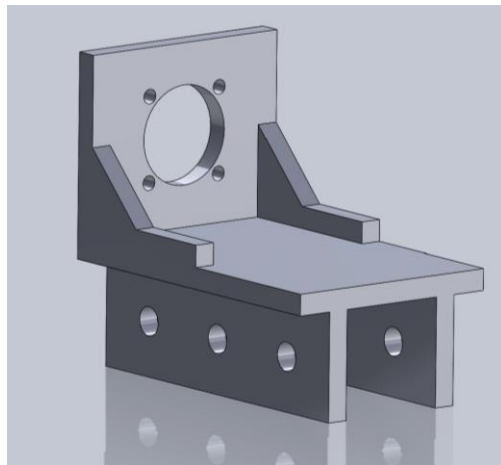


Figure 43: Second stationary motor mount designed to secure a single Planetary Gearbox Nema 17 stepper motor to the top of the t-slot beam

The upper trapezius muscle connects to the base of the neck which correlates to an area directly above the top of the plywood in our model. The first horizontal t-slot beam was fixed to this location and the motor for this muscle activation was placed there. The lower trapezius connects directly to the spinal plane and the serratus connects to several ribs. These connections would need to pass through holes in the plywood (and in the case of the serratus, the ribs as well) ensuring forces pull in the proper direction. On the backside of the board each linear attachment would need to be channeled down toward the base of the structure. Along the base underneath the plywood, the second horizontal t-slot beam was secured, and it would house the motors for both the lower trapezius and serratus anterior muscles.

Free Standing Motor Mounting Systems

In the case of both the supraspinatus and deltoid muscles, all connections ran between two or more moving bone structures. For this reason, we could not utilize a motor mount fixed to the rig and researched ways in which to actuate between two moving parts.

Design One: Nema 17 and Worm Gearbox

We developed the idea of mounting both motors to one of the moving parts. We determined that the exposed space around the humerus would make it a good spot for motor placement. We created two mounting systems for two motor options that would attach directly to the front and rear of the bone. The uneven shape of the bone made attachments difficult and required the creation of a device that fit snugly to the bone and created a flat plane for the motor mounts to attach to. We were able to model a block in two parts that would sandwich around the humerus with a cutout of the humerus in the center, shown in Figure 44. The block was oriented to ensure that when the humerus was in its initial position the bottom face was parallel to the ground and the narrow, side face was parallel to the spinal plane.

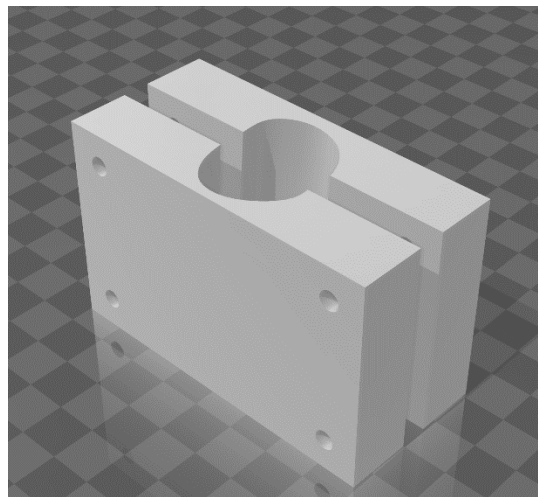


Figure 44: Two-part block with the humerus subtracted from the middle

The first design iteration for the motor mount shown in Figure 45 was designed for the Nema 17 Stepper Motors. Due to concerns with required torque, we incorporated a gearbox with a torque ratio of 60:1 achieved via a worm gear and worm wheel (Figure 45). The worm gear gearbox increases the torque and also prevents the system from being back driven. This would increase

the holding torque and allow the model to hold the humerus more easily at elevated positions throughout shoulder motion.

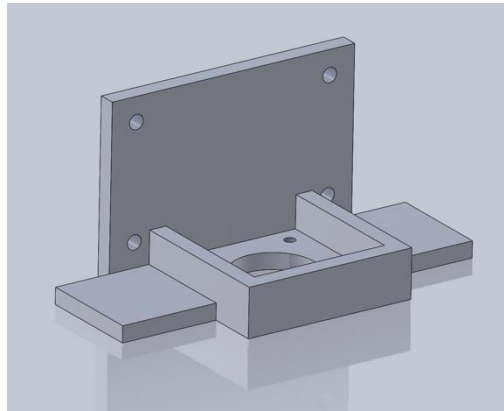


Figure 45: First design iteration in which the Nema 17 stepper motor sits upside down in the mount with the shaft directly inserted into a worm gearbox

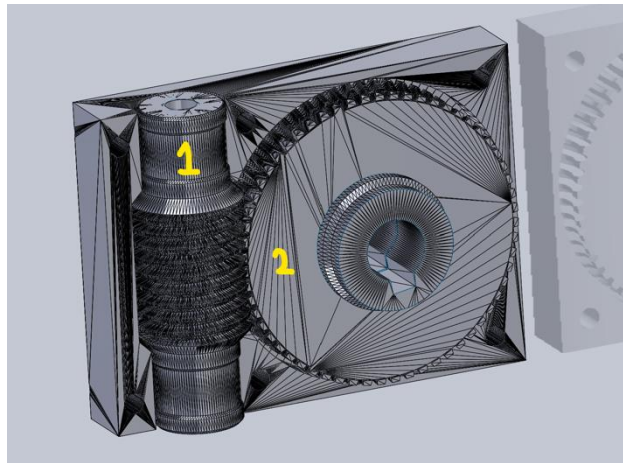


Figure 46: Exposed view of the gearbox with a worm gear and worm wheel in its casing

The dual mount assembly would include two motor mounts, one on either side of the humerus, bolted to the two-part humeral block. Either side would have the gearbox positioned directly below the motor with the worm gear directly connected to the motor shaft. The boxes would be rotated in opposite directions to ensure that shafts connected to the worm wheel were parallel to the board and ran along the interior and exterior of the humerus. The end of each shaft opposite the gearbox was secured via a small device attached onto the motor mount. The assembly is shown in Figure 47 below.

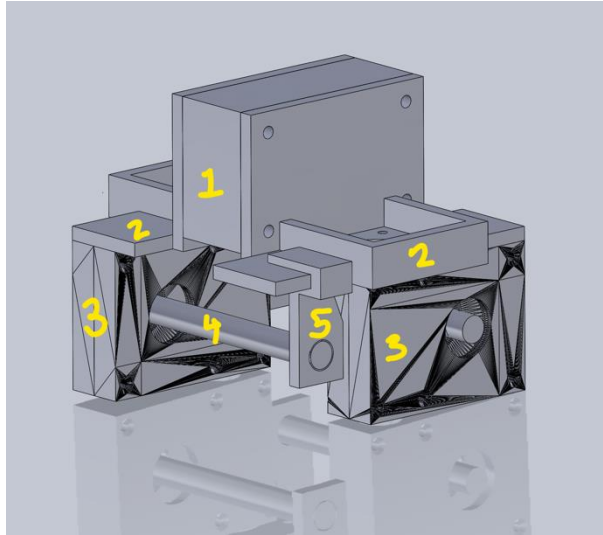


Figure 47: Assembly of humerus mounting block (1), stepper motor mounts (2), worm gear boxes (3), spool rods for spooling fishing line (4), and spool clips (5)

Design Two (Final): Planetary Gearbox Nema 17 Stepper Motor

The second and final motor mount design shown in Figure 48 was designed for the higher torque Planetary Gearbox Nema 17 Stepper Motor that would remove the need for the gearbox. These motors are slightly larger than the Nema 17 motors used in the first design and have a more complex shape which made modeling more challenging. The motor is almost entirely enclosed, aside from slots to prevent overheating, and is secured to the mount via the front circular face. The mount was designed to centralize the motor's center of mass along the central plane of the humerus.

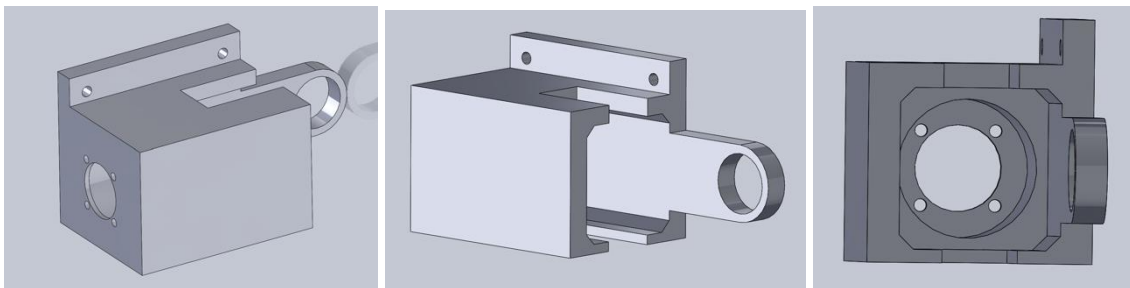


Figure 48: Final design for humerus motor mount housing one Planetary Gearbox Nema 17 stepper motor

Like the former mount design, both mounts would be bolted directly to the two-part block on the front and rear face of the humerus. A system needed to be developed to transmit the rotation at a 90-degree angle so that the shafts were parallel to the board and ran along the interior and exterior of the humerus. We chose to implement a pair of bevel gears, one of which would attach to the motor shaft and the other to the shaft that directly attached the muscle. Each of the two shafts would need to be secured on either side by a fixture and bearing resulting in the creation of an L-bracket designed to attach to the front of the motor mount on one end and house the shaft bearing on the other. The final assembly for the humeral mounting system is shown in Figure 49 below.

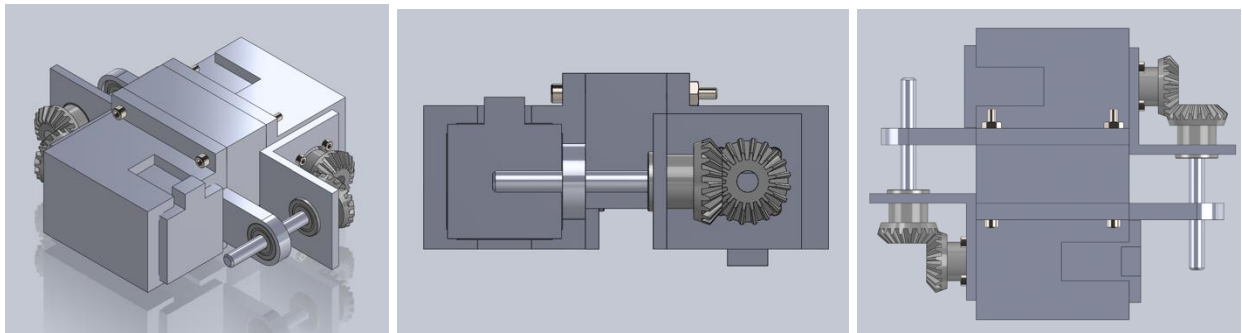


Figure 49: Complete design of assembly for free-standing motor mounting system

Manufacturing and Material Selection

Bone Modeling

When looking to purchase the bone model files from Biomedical Modeling Inc., we were offered the option of purchasing an anatomically correct full-scale 3D model file of the bones of the shoulder in the form of an STL file or a CAD file. The CAD file was more expensive at \$175 and was capable of being edited in SolidWorks once it was purchased. The STL file was cheaper at \$75. It is not possible to edit this file in SolidWorks but could be edited in an STL editor such as Blender and 3D Builder. We decided upon purchasing the STL file to provide more flexibility in our budget while still acquiring a 3D model we could work with.

We decided to 3D print the bones within our shoulder rig, including the scapula, humerus, clavicle, rib cage, and additional support elements. 3D printing was determined as the best manufacturing method for the bones, as bones are geometrically complex structures that are

easier to replicate using additive manufacturing rather than machining. We considered several different materials for bone creation including both FDM and SLA compatible 3D printing materials. We wanted to choose a material that had a bending strength, bending modulus, and elastic modulus that were like properties of bone. We were also looking for an affordable option. From the information shown in Table 1 below, we determined PLA filament and Rigid 10K resin to be the top two contenders for the best material. Rigid 10K has the closest match to that of humeral bone in terms of bending strength followed by PLA. However, Rigid 10k has a much higher elastic modulus than that of real bone, meaning it is much more brittle than true bone. Additionally, a more brittle material has a higher likelihood of fracturing when holes are being drilled into it, which would be problematic for our assembly process. The major factor when it came to deciding upon a material was price. Using Rigid 10k resin is roughly six times more expensive to print with than PLA. With a limited budget, we decided it would be best to use PLA for our material. We hope that a future team will investigate refining the material used to represent bone in this model.

Table 1: Bone vs 3D Printing Material Properties

Mechanical Properties	Bone (Humerus)	Rigid 10K	Rigid 4000	PLA	PETG	Polycarbonate
Bending Strength (MPa)	128.44	126	105	106	69	75
Bending Modulus (GPa)	2.35	9	3.4	3.5	2.1	1.88
Elastic Modulus (GPa)	3.73	10	2.1	1.3	2.1	2.13
Price/Gram	-	>\$0.18*	>\$0.10*	\$0.03	\$0.05	\$0.05
Available at WPI?	-	Y	Y	Y	N	Y

Note. Material properties of select 3D printing materials versus that of bone, specifically the humerus. Humerus materials properties are from a study by Mukherjee et al., 2011. *Cost estimate based on typical print density and cost per liter resin from FormLabs. (*MakerBot PETG 3D Printing Material | Heat, Chemical, Moisture Resistant*, n.d.) (Mukherjee et al., 2011) (*Build Strong Parts in Engineering Thermoplastic.*, n.d.) (*Using Rigid 10K Resin*, n.d.)

After deciding upon PLA for the bone material, different infill percentages were experimented with to see what would be best for our model. We wanted to achieve the highest strength and machinability while minimizing material use if possible. Low-infill PLA is not ideal for inserting fasteners, as there is less material for the fasteners to grip onto leading to weak connection points and structural instability. We ultimately went with 90% infill for all our 3D printed parts, as we found parts with lower infill were not easy to work with when attempting to drill holes and screw fasteners into them. For an infill pattern, we chose cubic as it is one of the strongest infill patterns (Arceo, 2021).

All the bones for our model were printed using the 3D printers in the WPI Prototyping Lab. Each bone's respective STL file was imported to the 3DOS software, where it was configured to have an optimal infill percentage, base supports, and printing angle. All of the bones were printed on either the Lulzbot 6 Taz or on the Ultimaker 3.

The humerus was the largest print of all the bones. Considering the long length of the humerus and the size of the 3D printers in the prototyping lab, we decided to slice the humerus in half, leading to two separate prints. Each half had a hole where the humerus was sliced so a pressure fit dowel could be inserted for additional support once the humerus was assembled (shown in Figure 52). Both ends of the humerus were printed using the Ultimaker 3. An image of the half and full 3D printed humerus can be seen below in Figures 50 and 51.

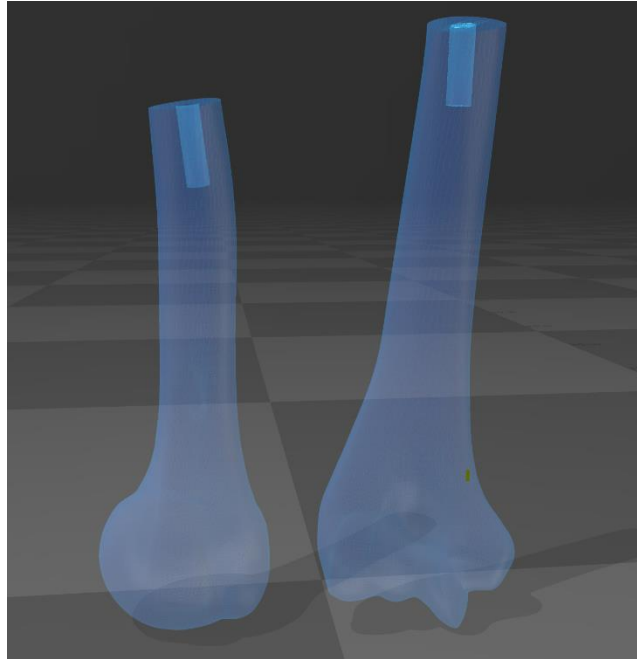


Figure 50: X-ray view of the top (left) and bottom (right) pieces of the humerus



Figure 51: 3D printed inferior (top) end of humerus

Once the two parts of the humerus were printed. The humerus was assembled using the pressure fit dowel and epoxy. An image of the full humerus can be seen below in Figure 52.



Figure 52: Full assembly of 3D printed humerus

The next bone that was printed was the scapula. The scapula was printed using the Lulzbot 6 Taz. An image of the scapula being printed, and the final print can be seen below in Figure 53.

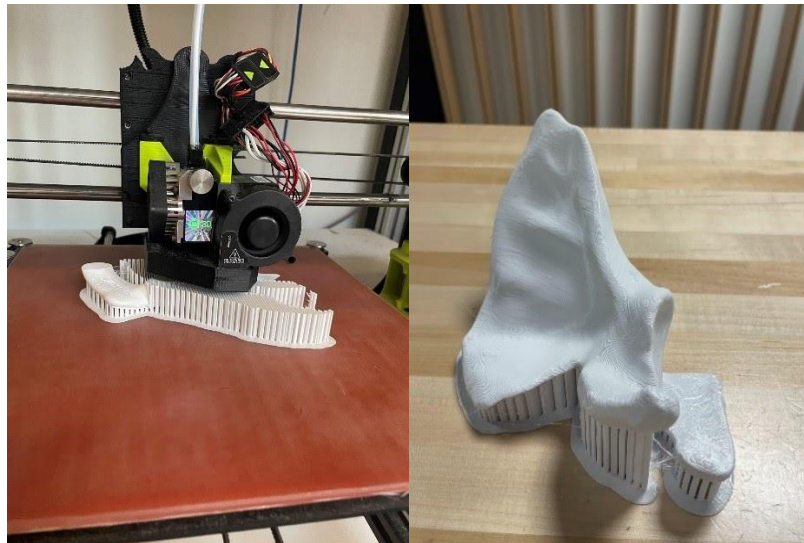


Figure 53: 3D print of scapula

The clavicle was the next bone to be printed. The clavicle was printed using the Ultimaker 3. An image of the final scapula print can be found below in Figure 54. After printing, it was connected to the ball joint linkage and attachment block that composes the sternoclavicular joint as shown in the final design. The clavicle assembly is shown below.

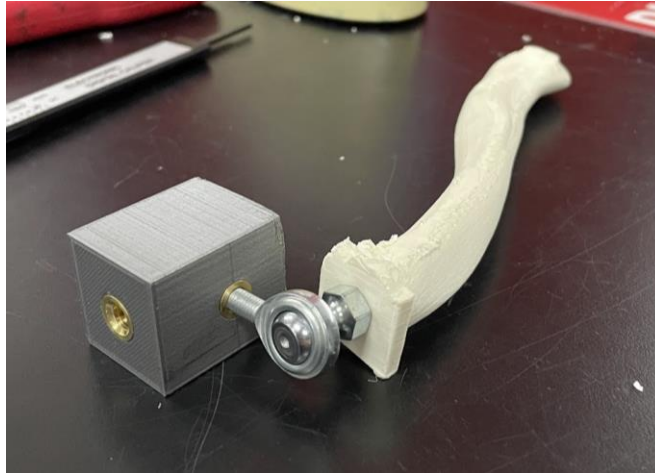


Figure 54: Assembled clavicle, ball joint linkage, attachment block, and heat press inserts

The ribs were the last bones that were printed. Each rib was individually printed either on the Ultimaker 3 or the Lulzbot 6 Taz. Below in Figure 55 an example of the one of the ribs that was printed can be seen, as well as the block connection point that was printed with each rib.

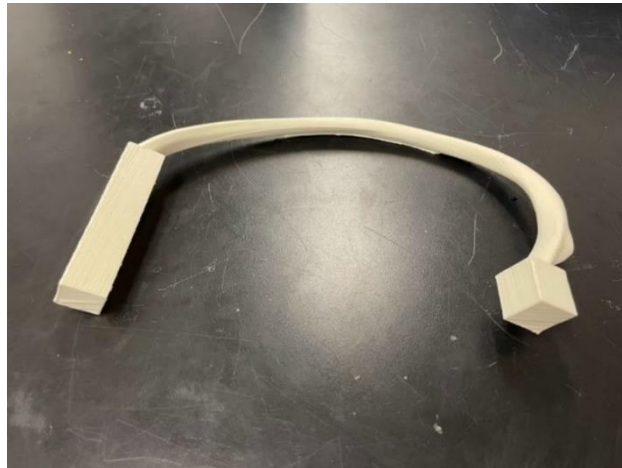


Figure 55: Final 3D printed version of Rib 5

Rig Assembly

The base support structure that was used in our model was composed of aluminum tri slot support beams connected by a sheet of plywood. The tri slot support beams formed two T-shaped legs that allow the model to stand and hold the plywood at a fixed position. The legs were made of two three-foot tri-slot beams that each stand vertically on a corresponding tri-slot support beam at their base. Each set of beams were supported using an L-bracket on one side and a steel

triangular support beam on the other. There were two additional beams installed connecting the two legs horizontally, one directly above the plywood and another parallel to the plywood along the base.

A 2ft by 4ft piece of 1in thick plywood was secured on either end to one of the vertical tri-slot support beams. This connection was made using bolts that extended directly through drilled holes in both the plywood and the t-slots. The plywood represents the spinal plane, all ribs and the clavicle were attached directly to it. To ensure proper orientation and spacing of all bones, the location of the connection points between each bone structure and the spinal plane were mapped out. Using the STL file of the overall rig shown in Figures 33 and 34, we were able to gather coordinates in the y-z plane for both ends of each rib and for the base of the clavicle. These coordinates were used to create the map shown below in Figure 56. This map was printed onto a large piece of paper and was directly transferred onto the plywood using Mod Podge.

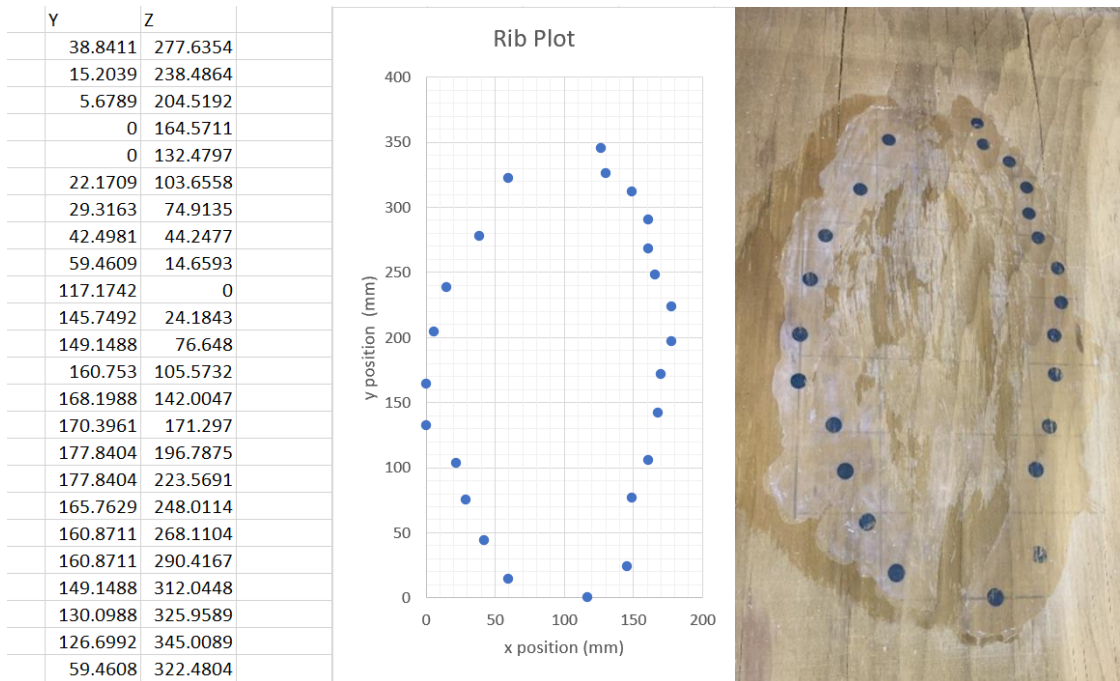


Figure 56: Table of rib connection points with its corresponding digital plot (left) that was transferred to the plywood (right) for accurate bone positioning

Once these locations were established, holes were drilled in the plywood at the marked connection points. Unlike the rib structures, the clavicle did not contact the board at the marked

location of its base due to the ball and socket joint design shown in Figure 54. The hole for the clavicle was instead drilled 1.18in in the positive y direction relative to the mapped base location. This ensured that the ball and socket joint aligned with the marked base location when the grey 3D printed structure in Figure 48 was bolted to the plywood. This clavicle structure and the ribs were fixed to the plywood by inserting threaded heat press inserts into the centers of the PLA blocks. Each of the press fits aligned with one of the drilled holes in the plywood. Bolts were inserted along the back face of the rig through the plywood and into the block to fasten the two together. The full assembly of the ribs on the plywood can be seen below in Figures 57 and 58.



Figure 57: Back of the assembly showing bolts from the rib connections, t-slot beam supports, and plywood

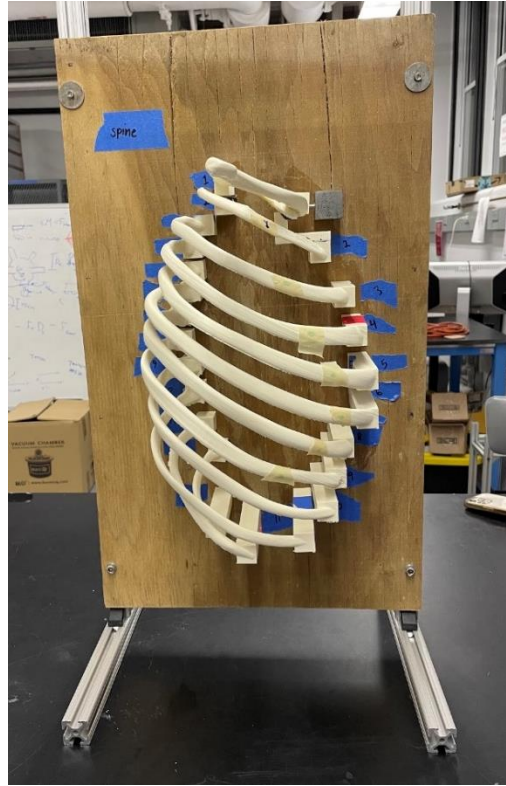


Figure 58: Right-side view of rib assembly

Replication of Muscles and Ligaments

It was determined that the best way to replicate forces exerted by the muscles of the shoulder was through mechanically actuated cables. This allows for a direct transfer of forces and measurable length contractions in the linear muscle attachments. A combination of braided nylon fishing line and elastic bungee cords was implemented to replicate the flexibility and support provided by the glenohumeral ligaments

Material Selection

The material properties of human soft tissue are incredibly complex with both contractile and elastic properties. We ultimately decided to forego pursuing accurate replication of soft tissue properties to simplify activation and force transfer within the system. The materials listed in Appendix C are options future teams may consider if there is an interest in more accurately replicating material properties of bulk soft tissue.

Ligaments

To replicate the acromioclavicular ligament capsule that connects the lateral end of the clavicle with the acromion on the scapula, highlighted in Figure 59, we utilized kinesiology tape on our final shoulder model shown in Figure 60. The KT tape successfully allowed the clavicle and scapula to articulate in their respective planes while also providing a limitation to the maximum amount of rotation allowed. The kinesiology tape is a compound material comprised of elastic, fibers, and adhesive glue. This was an ideal material for replicating the AC joint capsule as it allowed for flexibility within the joint, allowed for articulation of the clavicle and scapula, and adhered well to the PLA bone structures

In combination with the kinesiology tape operating to function as the AC joint capsule, a nylon monofilament was attached between the acromion and clavicle. Nylon fiber ligament was selected due to its extremely high strength and flexibility. Previous research looking to replicate bovine ligaments has focused on using nylon fibers in a braided strand for replacement surgery (Niehaus et al. 2013) (Sensini et al., 2019). The nylon monofilament fishing line selected to represent the muscles and certain ligaments in the model is rated to hold 150lbs. This monofilament was tied in knots repeatedly until a knot with a thickness of approximately 3mm was reached which is equivalent to the average reported thickness of the AC which acts as the cushion, spacer, and lubrication necessary to achieve motion between the clavicle and acromion of the scapula. This tied monofilament acts as the AC disc and allows for the clavicle and

scapula to maintain the same spacing during both translation and rotation, which is needed to achieve abduction at higher angles.



Figure 59: Anterior view diagram of ligaments and joint capsules that support the shoulder complex (Source: Vaskovic, 2022)

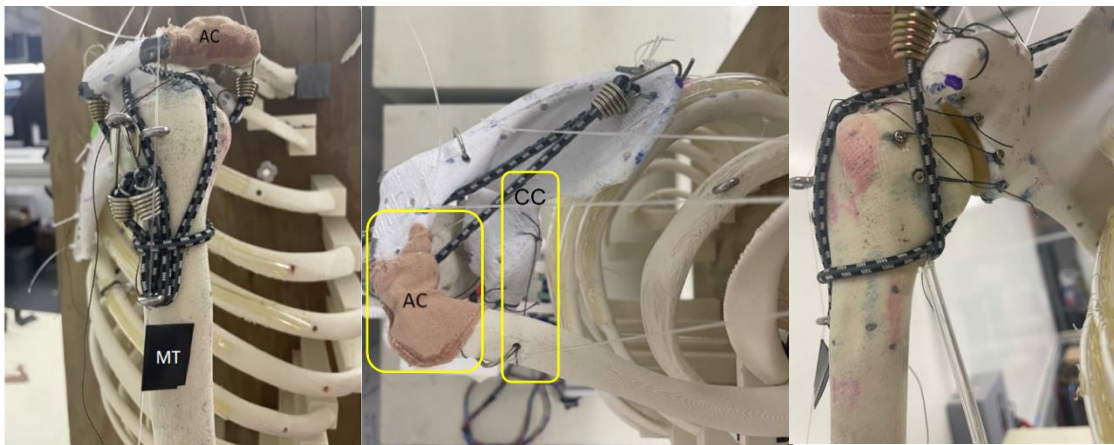


Figure 60: Side, top, and front view of shoulder model

To recreate the support and flexibility achieved by the ligaments, 3 bungee cords were used to connect between the scapula, clavicle, and humerus. The SGHL, MGHL, and IGHL are all responsible for the restriction of the movement of the shoulder to prevent dislocation which is why we used a more inelastic nylon cord to enforce the maximum displacement that the bungee cords alone would not be able to achieve. The same material was used to replicate the coracoclavicular ligament which is also pictured in the top right image of Figure 59. The

coracohumeral ligament is represented by the pathway of the bungee cord from the top of the humeral head to the scapula. While the attachment location of these bungee cords are not exactly anatomically accurate according to insertion and origin points, they are able to create the needed support and flexibility to replicate the movement of the shoulder forces because the direction of the force that provides stability is in the same direction. Having the elastic portion of the ligaments pass over the spot created support to hold the scapula to the humerus because it was under tension, which was not achievable with just the more inelastic braided fishing line.

Muscles

There are five primary actuators of shoulder abduction that we focused on: the upper trapezius, lower trapezius, middle deltoid, supraspinatus, and serratus anterior (Lam and Bordoni 2022). These muscles were replicated with the same nylon monofilament fishing line that was used to represent the AC ligament and linear muscles. The fishing line was tied in multiple holes that were drilled through the scapula at its anatomical insertion points. The fishing line is connected between the origin and insertion point of the muscle, with one end connected to the spool and motor and the opposite end fixed to the bone. In order to achieve abduction, the fishing line linearized the muscles a common method for analyzing the shoulder, like the elastic model in Figure 16 and the computer model in Figure 40. The fishing line was run throughout the model over the path of the linearized muscle and was fixed to the bone and attached to its corresponding motor. In the model the supraspinatus was run through a hole in the humerus at the location where the muscle attaches to create accurate moment arms when force is applied from the motor mounted on the humerus. For the serratus anterior and lower trapezius, the fishing line was fixed to the insertion point on the scapula and would run through holes in the wood board lined with soft plastic tubing to reduce friction and wear and tear on the line. Once the line is through the board, it connects to a motor mounted on the t-slot beam. While there are other muscles involved in shoulder motion and stabilization such as the rhomboids, pectorals, teres minor and major, levator scapulae, and latissimus dorsi, they are not necessary for shoulder abduction, our primary goal for our model.

To actuate the muscles the connection between the origin and insertion muscles needed to shorten in length. Our cable-winch system shortens the length of the muscle by pulling the fishing line through holes in the wood to motors on the opposite side of the wood from the

skeletal model or to the motors mounted on the humerus. The supraspinatus is actuated through the humeral head. It inserts on the edge of the scapula and travels through the top of the humeral head down to the motor where it winds up on the shaft. We acknowledge that the nylon monofilament fishing line will stretch over time causing a need for recalibration of the motors to have the muscles at the correct initial length, however other methods like cables that were inelastic were difficult to attach and were found to be too stiff to wrap around the spool or pass through the bends required to contract the serratus anterior, middle deltoid, and supraspinatus. Another reason the fishing line was selected was due to its low coefficient of friction, allowing for the line to glide over the PLA bone surfaces and through the silicone tubes that are used to guide the serratus anterior over the rib cage shown above in Figure 60. This is preferred to a metal cable that could potentially damage the plastic surfaces it would repetitively rub against.

Actuation System Implementation

Motor Selection

To begin our motor selection process, we performed a moment calculation on the humerus to gauge the maximum force required for muscle activation. We created the schematic shown in Figure 61 below to represent all the forces affecting rotational motion when the arm is abducted at 90 degrees. Table 2 details the variables used and includes values for the maximum moment calculation.

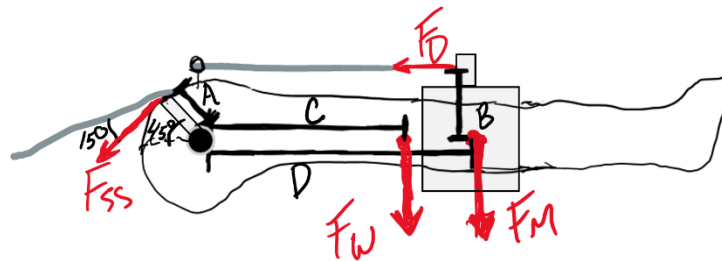


Figure 61: Force diagram used to calculate the moment of the humerus at 90 degrees abduction

Table 2: Variables Used in Moment Calculations

Variable	Description	Value at Max (90 deg)
A	Distance from supraspinatus insertion point to center of rotation of the humeral head	1 in

B	Distance from the central axis of the humerus to the axis to the line of action of the deltoid	1in
C	Distance from the center of rotation of the humeral head to the center of mass of the humerus	13in
D	Distance from the center of rotation of the humeral head to the location of the motors	11.25in
F _w	The weight of the 3D printed humerus	0.547lb
F _{ss}	Force of the supraspinatus	0lb
F _m	Weight of two Nema 17 motors	(0.88*2)lb
F _D	Force of the deltoid	27lb
θ	Angle of the humerus	90 deg

We performed the calculation during which the muscles would be required to provide that largest torque, at 90 degrees. The deltoid is the muscle that makes the largest contribution during abduction. In the hopes of acquiring a safe estimate of the maximum force required by any motor we performed the calculation with the assumption that the deltoid was the sole force acting to lift the arm. You will see this reflected in the equation below and in Table X where the force of the supraspinatus, the other major contributor in abduction, is set to zero.

Moment Equations

Condition: $\theta \leq 30$ (before scapulohumeral rhythm has begun)

Moment Equation:

$$\Sigma M = F_{ss}(A) + F_D(B) - 2F_m \sin\theta (D) - F_w \sin\theta (C)$$

Condition: $\theta \geq 30$ (after scapulohumeral rhythm has begun)

Moment Equation:

$$\Sigma M = F_{ss} \cos(.25\theta) (A) + F_D(B) - 2F_m \sin\theta (D) - F_w \sin\theta (C)$$

Maximum Moment Calculation

Moment Equation:

$$\Sigma M = F_{ss}(A) + F_D(B) - 2F_m \sin\theta(D) - F_w \sin\theta(C)$$

NEMA Motor Tests and Selection

Knowing the deltoid would need to pull approximately 27lbs of force, we established that a NEMA 17 would be the best motor to use for each muscle. Specifications about the NEMA 17 motors we used can be found in Appendix D.

Torque tests were conducted on the motors to check that they output sufficient torque. Unfortunately, the NEMA 17 motors we received ended up having a max torque of approximately 2.35 in. lbs. when the specifications listed a max torque of 3.98 in. lbs. For this reason, we decided to convert four of our five motors in our system to NEMA 17 motors with 27:1 planetary gearbox attached to ensure sufficient torque was achieved. The specifications for the 27:1 NEMA 17 motors can be found in Appendix D.

We attached spools on the ends of the motors to spool the fishing line around, which enabled the NEMA 17 motors to have very high maximum torques that would be more than sufficient to exert the necessary forces in the muscles. The theoretical maximum torque for each muscle motor is shown below in Table 3.

Table 3: Theoretical Maximum Motor Torque

Muscle	Motor Type	Spool Diameter (mm)	Maximum Torque (Nm)	Maximum Torque (in.lbs)
Supraspinatus	Planetary	8	375	3319.03125
Deltoid	Planetary	8	375	3319.03125
Serratus Anterior	Planetary	12	250	2212.6875
Upper Trapezius	Planetary	12	250	2212.6875
Lower Trapezius	Normal	8	13.88888889	122.9270833

Note: Planetary refers to the 27:1 gear ratio planetary Nema 17 motors. Normal refers to the Nema 17 motor without the gearbox.

Stationary Motor Mounting Systems

For muscles 1-3: Exact location of motor and method of attachment to T-slot, location and type of attachments to the bone, physical locations and pictures of them set up, printed w PLA

The three stationary mounted motors representing the serratus anterior, lower trapezius, and upper trapezius muscles were mounted to the t-slot beams as shown below in Figure 62 and 63. All components were 3D printed with PLA besides fasteners.



Figure 62: Serratus anterior motor mount (yellow) and lower trapezius (gray) shown with motors and fishing line spools installed



Figure 63: Upper trapezius motor and mount shown from the front side of the board (left) and the back side of the board (right)

Humerus Motor Mounting Systems

The motor mounting system holding the motors representing the deltoid and supraspinatus is shown below in Figure 64. All components were 3D printed with PLA besides fasteners.

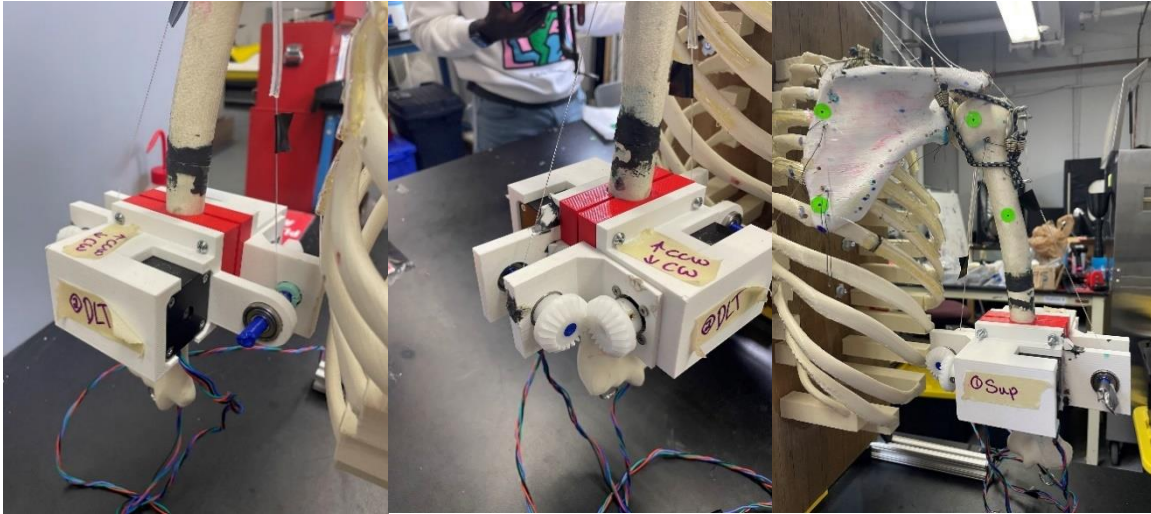


Figure 64: Several views of fully assembled humerus motor mounting system

Completed Model

The picture below in Figure 65 shows the completed model, showing all electronics, motors, bones, and support structures.

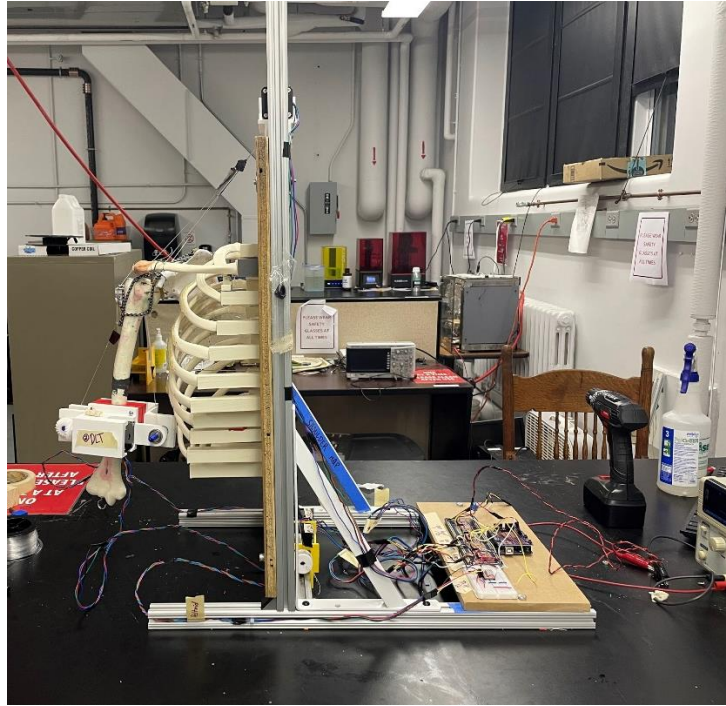


Figure 65: Fully Assembled Shoulder Model

Motor Circuitry and Motion Programming

To run the motors in a way that simulated muscle activation during abduction, we used an Arduino Uno microcontroller to control all five motors at once. A4988 stepper motor drivers were used to control each of the motors. The schematic for the circuit we used can be seen in Figure 66 below, and the actual circuit can be seen in Figure 67.

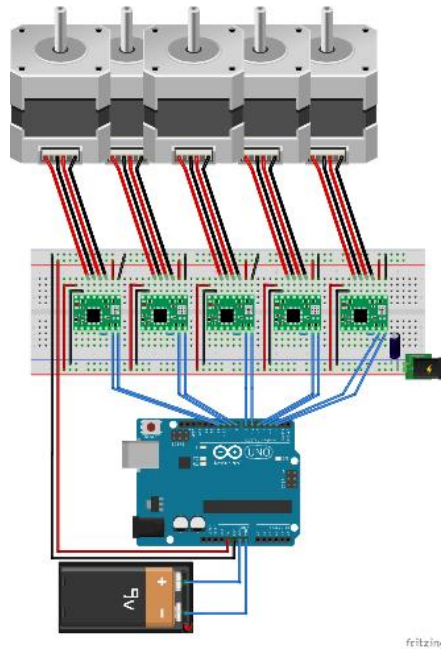


Figure 66: Motor circuit schematic

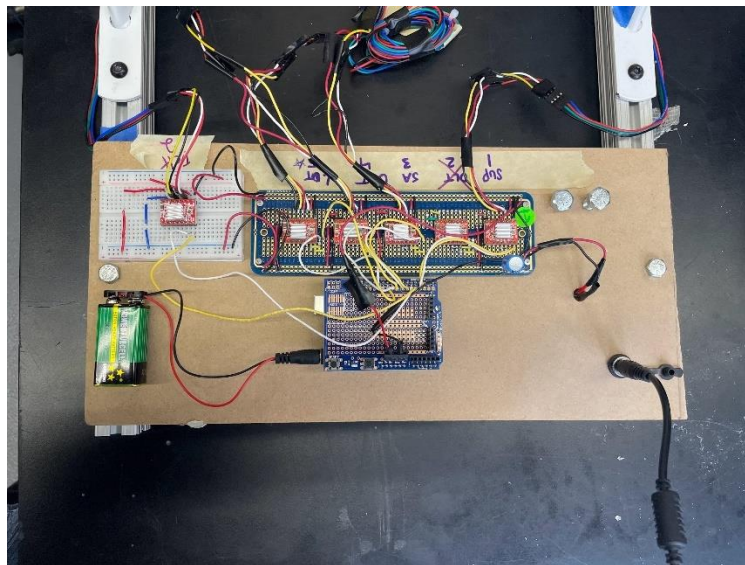


Figure 67: Fully assembled physical circuit

The code to run the motors considers motor steps per revolution, spool diameter, the total distance each muscle must move during abduction, the activation start time of each muscle, and the total desired movement duration. These variables are input into an Excel spreadsheet that outputs a block of code to be copied into a set of Arduino code to run the motion of abduction

based on the variable inputs. The activation start time for each muscle was determined based on a study conducted in 2010 regarding the order and onset time of muscle activation during shoulder abduction and adduction. According to the study, the order of activation of the muscles we included in our model are the supraspinatus, the deltoid, the serratus anterior, the upper trapezius, and the lower trapezius (Wickham et al., 2010). The onset times in the study were based on a 24 second abduction motion. The muscle onset times were scaled for our model based on the total desired duration of the motion. The total change in length of each muscle was determined by measuring the distance each fishing line traveled when the shoulder was manually moved from the initial position to the 90-degree abducted position. The calculated change in length of each muscle is shown in Table 4 below.

Table 4: Change in Length of Linearized Muscles During Abduction

Muscle	Change in Length (mm)
Supraspinatus	39
Deltoid	47
Serratus Anterior	19
Upper Trapezius	32.8
Lower Trapezius	20

Testing

To test our rig’s ability to achieve our goals, we ran three trials where the model was programmed to execute three abduction and adduction cycles per trial. Four photo-tracking dots were placed on the model – two on the scapula, and two on the humerus as seen in Figure 68 below.



Figure 68: Example of photo tracking dots used in testing

Before each trial began, the rig was moved to its initial position with the humerus resting vertically alongside the ribcage. The relative positioning of the primary bone structures was defined by measurements taken within the STL file. Orientation of the bones relative to the stationary board was replicated on the physical rig and this was defined as the initial position. An iPhone 13, with 60 fps, mounted on a t-slot beam was used to take a video recording of each trial so that scapulohumeral rhythm could be tracked based on the tracking point locations. The model was programmed to perform abduction over a 24 second period, pause for one second, then perform adduction to return to its initial position over 24 seconds. Each 49 second period is considered one “cycle”. This cycle was repeated three times per trial. After each trial was completed, the position of the four photo-tracking dots were measured to compare their positions with the goal initial position.

Results

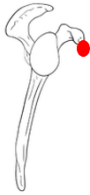
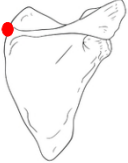
Goal One: Accurate Positioning of the Scapula

Using the STL file assembly, we were able to establish a coordinate system centered at the top left corner of the board and determine the exact coordinates of three anatomical points on the scapula (see Table 5 below). Our goal was to determine the accuracy of the model’s return to initial position after performing abduction. Accuracy was defined as being within 5mm of its initial position in any of the three dimensions within our chosen coordinate system. We

conducted three trials each starting from the initial position and cycling through the 24 second abduction three times. Following each trial, deviation of each point from initial position was measured in three dimensions. Using multiple measuring tools, we were able to determine each point's distance from the front face of the board (x-direction), distance from the left edge of the board (y-direction), and finally the distance from the top of the board (z-direction). Table 6 below lists the initial position measurements for all three points chosen along with their average deviation among the three trials. Aside from one outlier (9mm) no one measurement in 3D varied from the desired value by more than 5mm.

The magnitude of displacement vectors was calculated, and the average deviation was determined to be within 2% of the expected value. Because measurements were taken manually, we will assume that due to human error the average is within 5% of the expected value. To improve upon this measurement technique, future teams could consider the implementation of more advanced photo tracking methods that would enable the calculation of position in three dimensions digitally.

Table 5: Average Deviation from Initial Position

Point	X	Y	Z	Location
1 (bottom tip of scapula)	99.18 mm + 1.33mm	78.5mm + 2.33mm	-296.0mm + 3.33mm	
2 (bottom tip of the coracoid process)	161.39 mm + 0.33mm	197.0mm + 5.67mm	-189.0 mm - 1.67mm	
3 (interior, upper edge of the scapula)	80.57 mm + 1.00mm	108.0 mm + 3.33mm	172.0 mm + 3.67mm	

Note: The +/- values above indicate the average deviation from initial position calculated based on the three trials. The images on the far-right show three points of consideration that were located within the STL file and transferred to the actual model to ensure consistent and accurate initial positioning of the scapula.

Goal Two: Achieve Desired Range of Motion

Part of our goal was for our model to achieve a full 90-degree rotation of the humerus. Examining the video footage of 13 cycles allowed us to identify the exact moment at which our model reached its maximum rotation. Each of the frames were examined and the angular displacement was calculated. The values recorded ranged between 56 and 63 degrees and fall outside our defined success range of within 5-10 degrees of the 90-degree goal. The scatterplot

below in Figure 69 shows the culmination of the maximum humeral angular displacements for each of the 13 cycles.

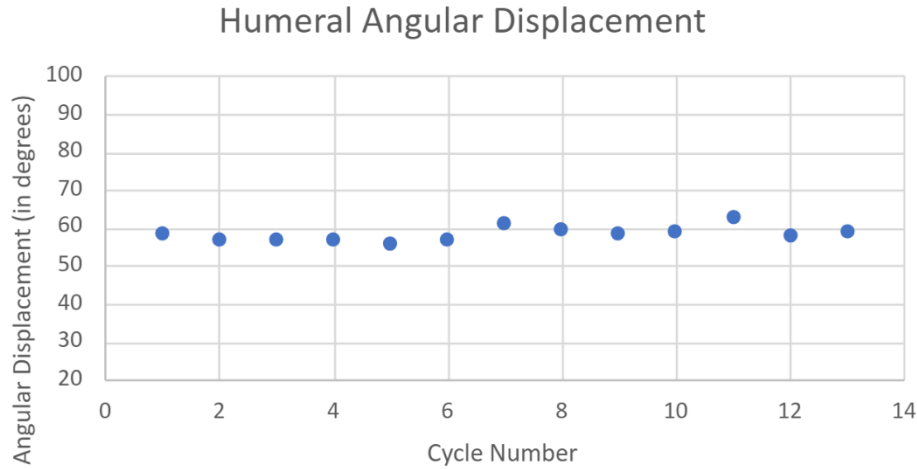


Figure 69: Resulting maximum angular displacement achieved by the humerus during abduction

Goal Three: Accurate Relative Motion

To determine whether we achieved accurate relative motion between the humerus and scapula we used video footage from a total of 13 cycles. Using the two pairs of position tracking dots located on the humerus and scapula, we were able to examine frames at regular intervals throughout abduction to record their respective angular displacements. Measurements of angular displacement of the scapula were taken at five intervals throughout abduction when the angular displacement of the humerus (in degrees) was 0, 30, 40, 50, and maximum. Based on these humeral angle changes, we were able to establish an expected set of scapular angular displacement values and compare them to the experimental values measured. We determined our success range to be within 5 degrees of where the scapula should be at any given point throughout the motion. The expected angular position of the scapula relative to the angular position of the humerus during abduction is graphed in Figure 70 below. The blue line represents the expected angular trajectory of the scapula during a full 90° abduction and the orange trendline shows our experimentally determined values. The graph has four major clusters of

orange data points located at 30, 40, 50, and 60 degrees of the humerus. These indicate the four positions, after zero, at which the scapula angle was measured relative to the humerus.

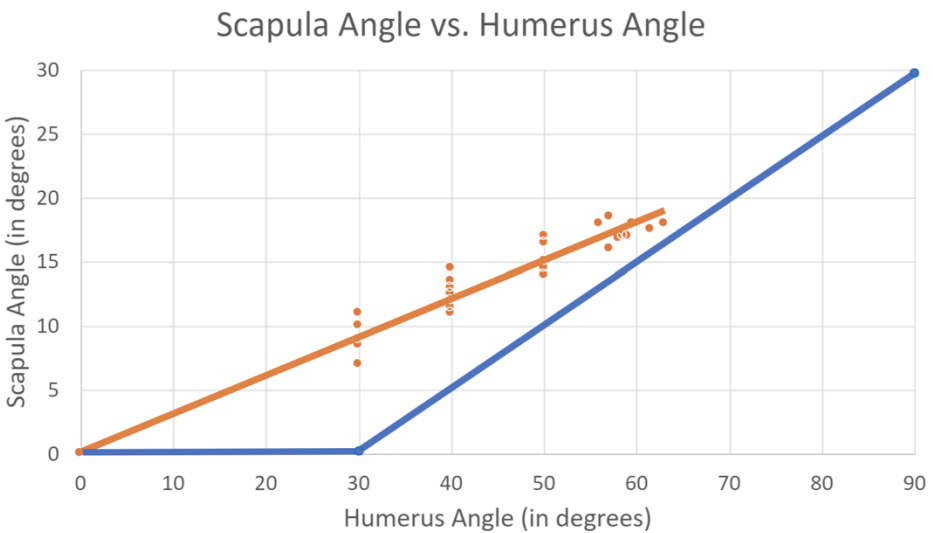
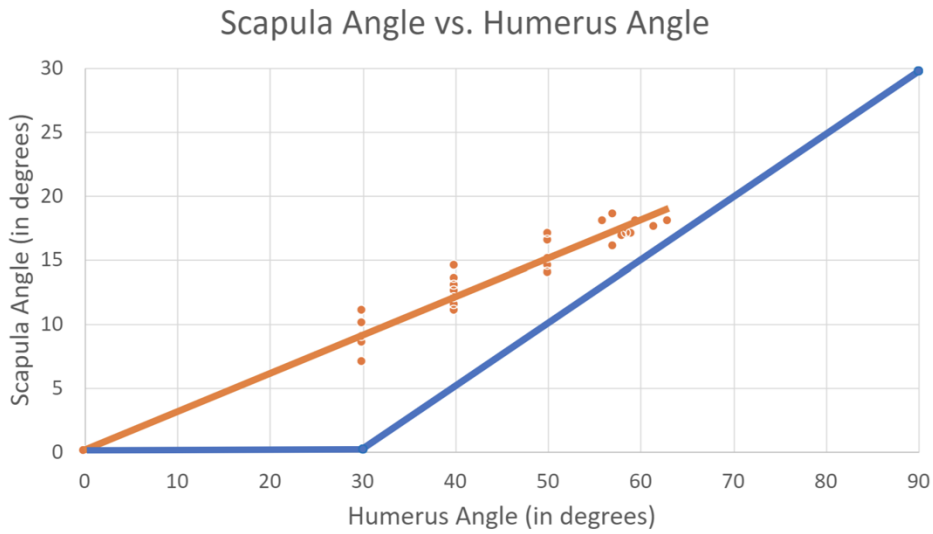


Figure 70: Relationship between the angle of the scapula and the angle of the humerus during abduction

As seen in the graph, the experimental values are fit well by the linear trend line for the 60° abduction and do not hold fast for the first 30 degrees of humeral rotation. Additionally, the relationship indicated by the trendline is not aligned with the expected line shown in blue. The

results do indicate a linear relationship between the two bone structures; however, the relationship begins 30° too soon and does not have the correct slope.

Discussion

After reviewing the results, we were able to define our successes and shortcomings. Model creation was a success as well as overall implementation of select ligament and muscle groups. One of the primary successes was achieving Goal One or the accurate positioning of the primary bone structures, specifically the scapula. Measurements after each of the four trials indicate that the three points on the scapula varied on average 4mm after performing three cycles of abduction. This very small displacement suggests that the model can perform functions and return to a start position that maintains anatomically accurate positioning. Steps should be taken in the future to improve the accuracy of these measurements through multi-angle photo tracking or a similar digitized process.

The following two movement goals fell short of our defined goal ranges for a number of reasons. The model was unable to achieve the desired range of motion, and ultimately reached a maximum that was about 2/3 of the goal range. Similarly, the third movement goal of replicating scapulohumeral rhythm didn't quite make the mark. Experimental values regarding angular positioning of the humerus and scapula followed a linear relationship, however, this relationship was closer to a 3:1 ratio vs the expected 2:1 seen within the human body. Also, the expected delay in scapular movement during the first 30 degrees of abduction, which is a crucial part of scapulohumeral rhythm, was nonexistent.

There were several contributing factors discovered in the testing phase that likely contributed to the differences between expected values and experimental outcomes. After several testing cycles, we noticed a slight stretch beginning to occur within our linear muscle attachments. Although the fishing line was incredibly strong it was too ductile and plastically deformed under the forces of the motor. To ensure a more direct force transfer and achieve the desired range of motion it is crucial to reduce the ductility of muscle attachments. Also contributing to the model's restricted range of motion was the humerus' deviation from the desired plane. The image in Figure 71 below of the model during testing shows that the humerus has deviated from the plane perpendicular to the board. Potential causes include uneven distribution of the upper trapezius

and exclusion of stabilization muscles that connect to the front and back of the face of the humerus.

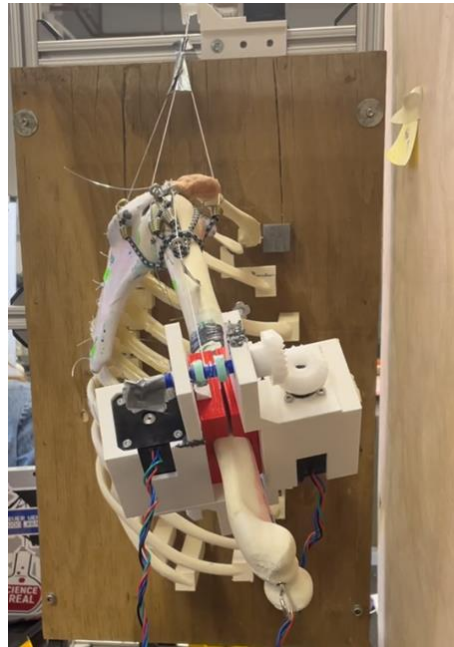


Figure 71: Image showing humerus' deviation from the desired plane

Lastly, we made the decision to use the Nema 17 stepper motors with 27:1 torque ratio increase for all of the muscle groups except for the lower trapezius. During testing it became clear that the regular Nema 17 used for the lower trapezius did not have enough torque. The lack of torque could have contributed to the scapula's inability to remain stationary for the first 30 degrees of abduction. It is also possible that muscle onset times were inaccurate, leading to the model's deviation from scapulohumeral rhythm.

Conclusion and Recommendations

This project set out to build a model shoulder that could achieve abduction with accurate relative motion between the bones of the shoulder. We were able to achieve this to an extent, with much room to improve. The model included anatomically accurate bone structures with a series of linear attachments. Although the model did not achieve the desired range of motion, our activation system succeeded in abducting the arm and creating simultaneous motion of the scapula. We were able to achieve accurate positioning of our primary bone structures and a

strong linear relationship between scapular and humeral motion. This relationship deviated from the expected values but still maintained linearity and moderate strength.

We hope that future teams will take our model and improve upon it. There are several aspects of the model that could be improved. One aspect would be motion accuracy. This could be achieved through better material use for the muscles and by fine tuning the positioning of bones, ligaments, and any other biological parts deemed necessary to achieve biomechanical accuracy in the model. Another aspect would be tissue material. We used PLA for the bones in our model, which had some properties that made it like bone, but it is certainly not the best material for replicating the material properties of bone. Similarly for the muscles, we did not attempt to replicate their material properties. A future team could research potential materials that better replicate the complex viscoelastic properties of muscle tissue to then implement in the model. Another aspect is expanding the possible motions the model can achieve. We focused on achieving strictly abduction. With the implementation of more muscles and programming, a future team could enable the model to execute multiple shoulder movements. A final aspect would be optimizing the design for easy assembly and replication to potentially sell as a commercial product. Our team sees the potential for this model to be sold as an educational product to educational and medical institutions and would like to see future teams continue the development of this idea. A future iteration of the model with representative muscles and ligaments could be used for injury and injury prevention studies.

Broader Impact

Our background research suggests that current realistic shoulder models do not properly replicate shoulder motion to its fullest extent. By creating a shoulder model that closely replicates the human shoulder's anatomy and physiology, more people will be able to better understand the shoulder and all the complex factors that go into shoulder motion.

Engineering Ethics

The American Society of Mechanical Engineering code of ethics states principles and canons that reflect upon what it means to be withhold integrity as a Mechanical Engineer. The fundamental principles that our project resonates with are:

- a. Using their knowledge and skill for the enhancement of human welfare
- b. Striving to increase the competence and prestige of the engineering profession

The fundamental canons our project resonates with are:

- c. Engineers shall hold paramount the safety, health, and welfare of the public in the performance of their professional duties.
- d. Engineers shall perform services only in the areas of their competence.
- e. Engineers shall associate only with reputable persons or organizations.
- f. Engineers shall consider environmental impact in the performance of their professional duties.

Throughout the duration of our project, our team took several steps to ensure that our work was held to a high standard of engineering ethics. Before any major developments were made with our model, we spent time conducting extensive research on the human shoulder and realistic shoulder models. Having a strong understanding of the anatomy and physiology of the human shoulder was a crucial first step in our project. Understanding how our model could be implemented into the classroom and in medical practices would provide a resource to educate a large population of people on the structure and function of the shoulder. When developing our model, we ensured that our design was original work, and was different from existing models. Lastly, an important aspect of our model that we considered was the environmental impact of our product. Our product is intended to be easily assembled and reusable.

Social and Global Impact

This model could be implemented in educational settings. Whether that educational setting is a elementary school classroom or in a medical school, this model would allow medical professionals, patients, and students to visually learn about the structure, function, and motion of the shoulder. Currently, anatomical studies are taking place using human cadavers. Cadavers provide excellent anatomical visualization, but they are limited in showing function. The model that we have created provides users with the opportunity to analyze many factors that go into shoulder structure and motion. This model could also be used within medical practices. Physical therapists and doctors could use this model when working with their patients. They would be able to show their patients how their shoulder works and the areas of the shoulder that they might be targeting to heal after a shoulder injury occurs. This model could also be implemented in injury prevention and the design of protective devices. Shoulder injuries are common during high

impact scenarios and there is certainly an opportunity to use a realistic physical shoulder model for injury studies and in the design of protective devices.

Environmental Impact

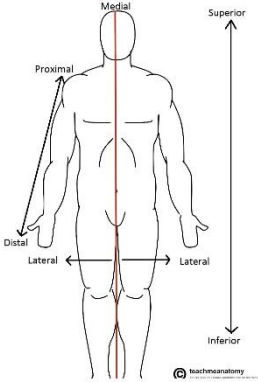
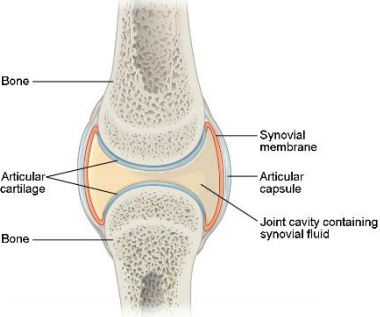
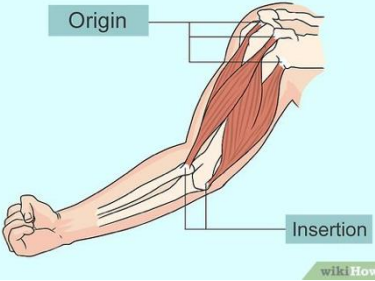
While developing this model, our team considered how we would be able to create a model that would be environmentally friendly. The bones in our model are all 3D printed out of Polylactic Acid (PLA), which is a material that is biodegradable and breaks down within 12 weeks. We also used scrap wood as part of our prototype, enabling the production of our model without purchasing any wood products.

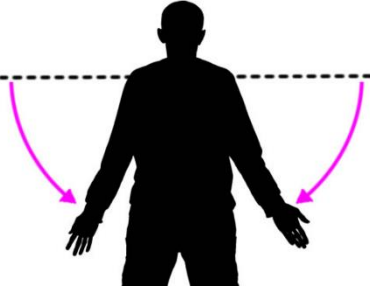
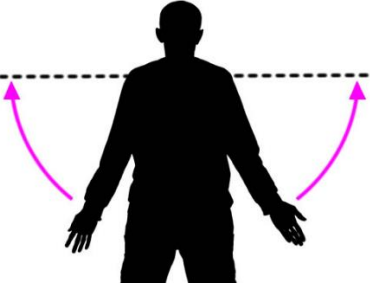
Economic Impact

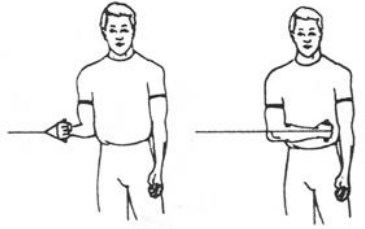
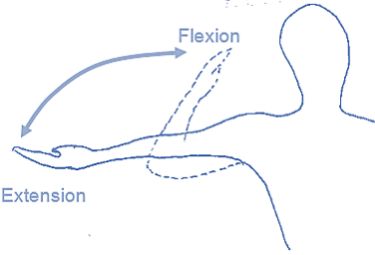
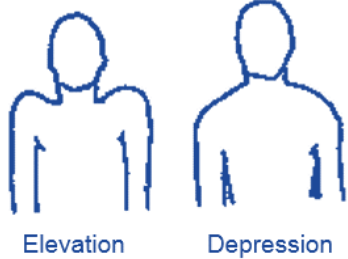
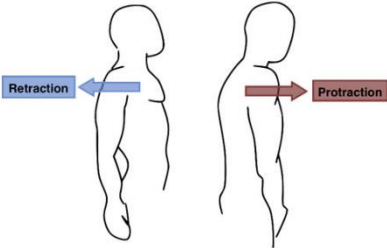
The relative cost to a consumer is mainly materials and components of our model. The material that was used to 3D print the bones in the model was inexpensive. The cost of the stepper motors and other hardware used within the model will contribute to the overall price of the model. The overall price of this model would be much cheaper than standard educational models that have been used previously in medical institutions.

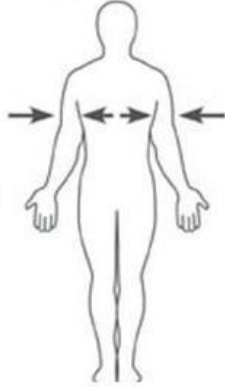
Appendices

Appendix A: Anatomical definitions/terms

Term	Definition	Supporting Image
Superior	Toward the head/upper end of the structure	
Inferior	Away from the head: lower	
Medial	Towards the midline	
Lateral	Away from the midline	
Articulation	Where two bones are connected	
Origin	Attachment of a muscle to a more stable bone, a fixed point that doesn't move during muscle contraction	
Insertion	Point of attachment in a muscle where more movement occurs, a point	

	that moves during muscle contraction	
Flexion	Decreasing the angle between two bones (bending)	
Adduction	Movement of a limb or other part toward the midline of the body or toward another part	Adduction 
Abduction	The movement of a limb away from the midline of the body	Abduction 

<p>Internal Rotation/Medial Rotation</p>	<p>Rotational movement towards the midline</p>	
<p>Extension</p>	<p>Increasing the angle between two bones (straightening a bend)</p>	
<p>Depression</p>	<p>Downward movement, opposite of elevation</p>	
<p>Protraction</p>	<p>Movement of a body part towards the front of the body</p>	 <p><small>Image Credit: Wiki User: Osteomyoamare. License CC BY 3.0. commons.wikimedia.org/wiki/File:Protraction_Retraction.png</small></p>

<p>Superficial</p>	<p>Locating structures on or near the surface of the body</p>	<p>superficial</p> 
<p>Axial Skeleton</p>	<p>Forms the central axis of the skeleton, includes the bones that form the skull, laryngeal skeleton, vertebral column, and thoracic cage</p>	

Appendix B. Schematics for Soft Tissue Attachments

Back View of Soft Tissue Attachments Layer 1

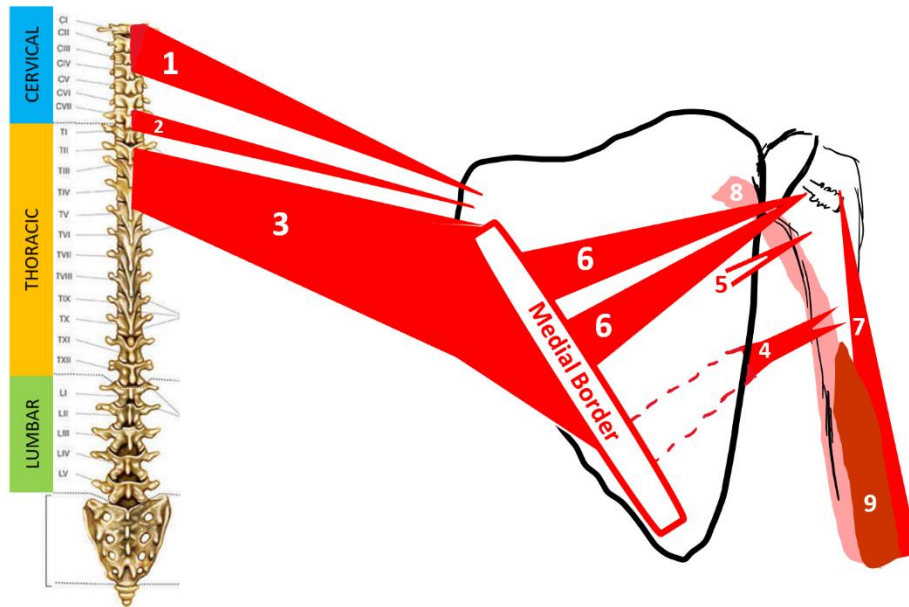


Table of Soft Tissue Attachments Pictured

	Component	Spinal Attachments	Scapula Attachments	Humeral Attachments
1	Levator Scapulae	C1-C4	Top, Medial corner	NA
2	Rhomboid Minor	C7-T1	Top, Medial corner	NA
3	Rhomboid Major	T2-T5	Medial Border	NA
4	Teres Major	NA	Lateral Border inferior angle	Medial lip of bicipital groove on the anterior

				surface of the humerus
5	Teres Minor	NA	Lateral Border	Greater tuberosity
6	Infraspinatus	NA	Infraspinatus fossa of scapula	Posterior of humeral head
7	Triceps Brachii: lateral head	NA	Posterior surfaces of the humerus below radial group	-posterior surfaces of the humerus - Olecranon process of ulna;
8	Triceps Brachii: long head	Infraglenoid tubercle	NA	-Infraglenoid tubercle Olecranon Process
9	Triceps Brachii: Medial Head	NA	Coracoid Process	-Anterior medial shaft of humerus

Back View of Soft Tissue Attachments Layer 2

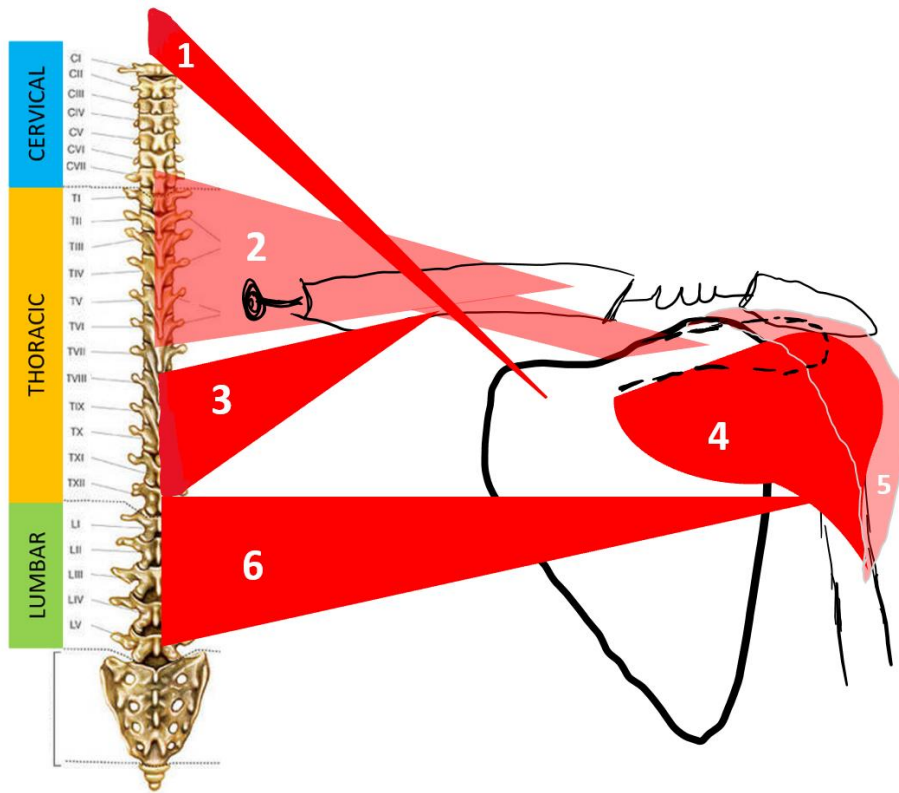


Table of Soft Tissue Attachments Pictured

	Component	Spinal Attachments	Scapula Attachments	Humeral attachments
	Trapezius			NA
1	-Upper Trapezius	Occipital	Top, Medial corner	NA
2	-Middle Trapezius	C7-T7	Medial edge of acromion, posterior part of lateral 1/3 of clavicle	NA

3	-Lower Trapezius	T8-12	Medial region of scapula	NA
4	-Middle Deltoid	NA	Acromion Process	Deltoid Tuberosity
5	-Posterior Deltoid		Spine of Scapula	Deltoid Tuberosity
6	Latissimus Dorsi	T7-L5, posterior surface of the sacrum, iliac crest, and lower three ribs	NA	Medial floor of bicipital groove of the humerus

Front View of Soft Tissue Attachments Layer 1

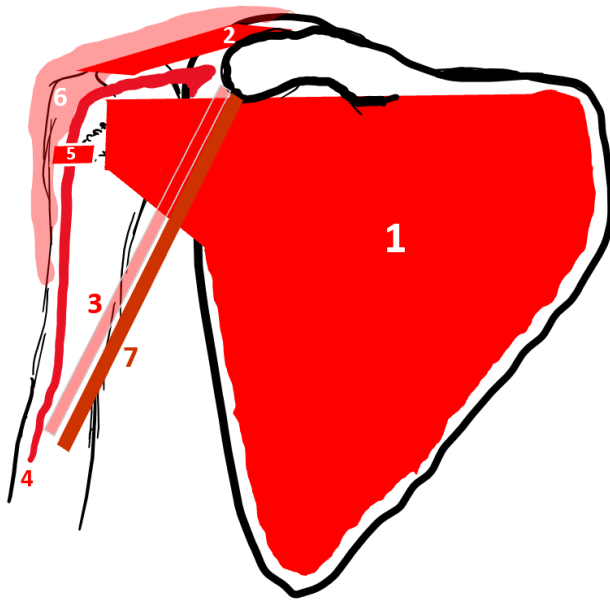


Table of Soft Tissue Attachments Pictured

	Component	Scapula Attachments	Humeral Attachments	Clavicle Attachment
1	Subscapularis	Front face	Anterior of humeral head	NA
2	Supraspinatus	Superior Border	Superior of humeral head	NA
3	Biceps Tendon Short Head	Coracoid Process	Radial tuberosity of the radius	NA
4	Biceps Tendon Long Head	Supraglenoid tubercle of the scapula	Radial tuberosity of the radius	NA

5	Transverse Humeral Ligament	NA	Greater Tuberosity to Lesser Tuberosity	NA
6	Anterior Deltoid	NA	Deltoid Tuberosity	Lateral third of clavicle
7	Coracobrachialis	Coracoid Process	Bicipital aponeurosis to the fascia on the medial side of the forearm	NA

Front View of Soft Tissue Attachments Layer 2

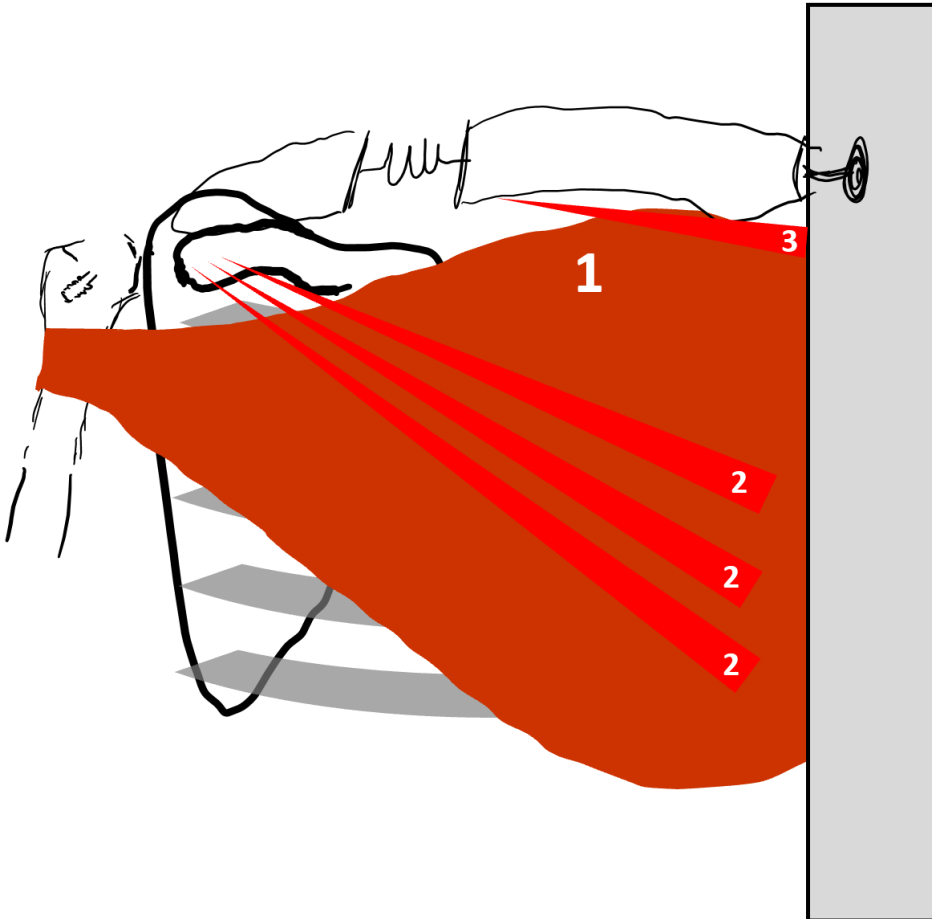


Table of Soft Tissue Attachments Pictured

	Component	Scapula Attachments	Humeral Attachments	Sternum/Rib Attachments	Clavicle Attachments
1	Pectoralis Major	Inferior axillary border near the inferior angle	Lateral lip of the bicipital groove of the humerus	Sternocostal head- lateral manubrium and sternum, six upper costal cartilages and	NA

				external oblique aponeurosis	
2	Pectoralis Minor	Medial border and coracoid process	NA	Ribs 3-5	Medial 3 rd of clavicle
3	Subclavius	NA	NA	Rib 1 at the connection with the sternum	Medial, underside of clavicle
4	Costoclavicular Ligament	NA	NA	Rib 1	Medial, underside of clavicle
5	Interclavicular ligament	NA	NA	Top medial edge of the clavicle	Central sternum

Side View of Serratus Anterior Attachments

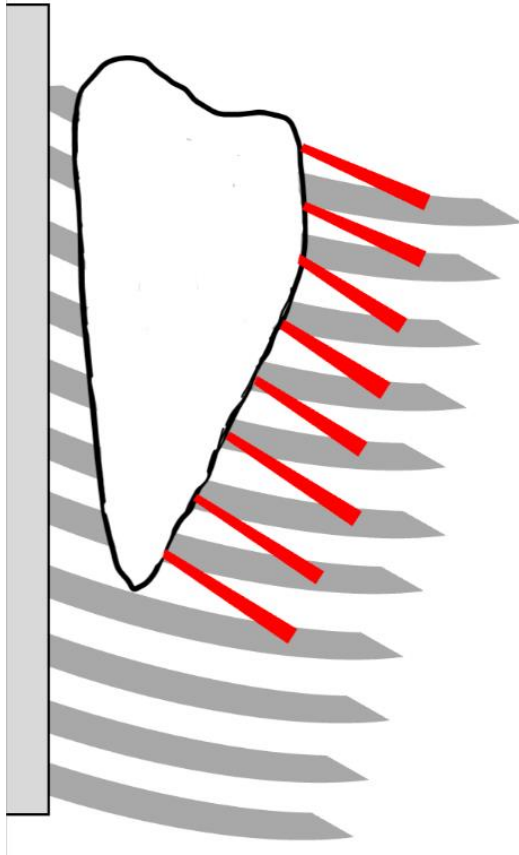


Table of Soft Tissue Attachments Pictured

	Component	Scapula Attachments	Thoracic Attachments
1	Serratus Anterior	Anterior surface on medial border	Ribs 1-8 anterior intercostal membranes from midclavicular line

Front View of AC Attachments

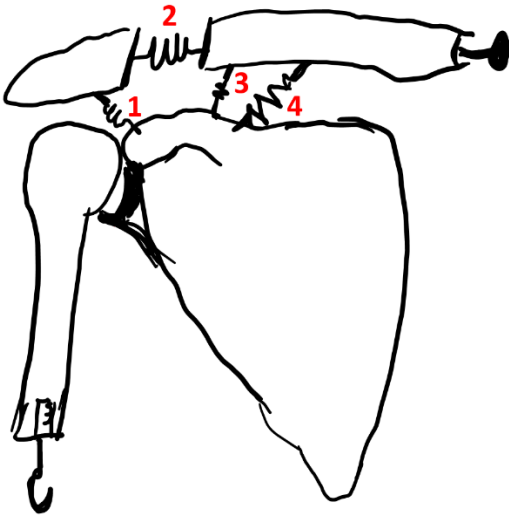


Table Front View of AC Attachments

	Component	Scapula Attachments	Clavicle Attachments
1	Coracoacromial Ligament	-Acromion of scapula -Coracoid Process	NA
2	Acromioclavicular ligament	Acromion	Acromial End
3	Trapezoid ligament (Coracoclavicular) Conoid ligament (Coracoclavicular)	Coracoid Process	Trapezoid Line

4	Conoid ligament (Coracoclavicular)	Coracoid Process	Conoid Tubercle
---	---------------------------------------	------------------	-----------------

Glenohumeral Ligaments

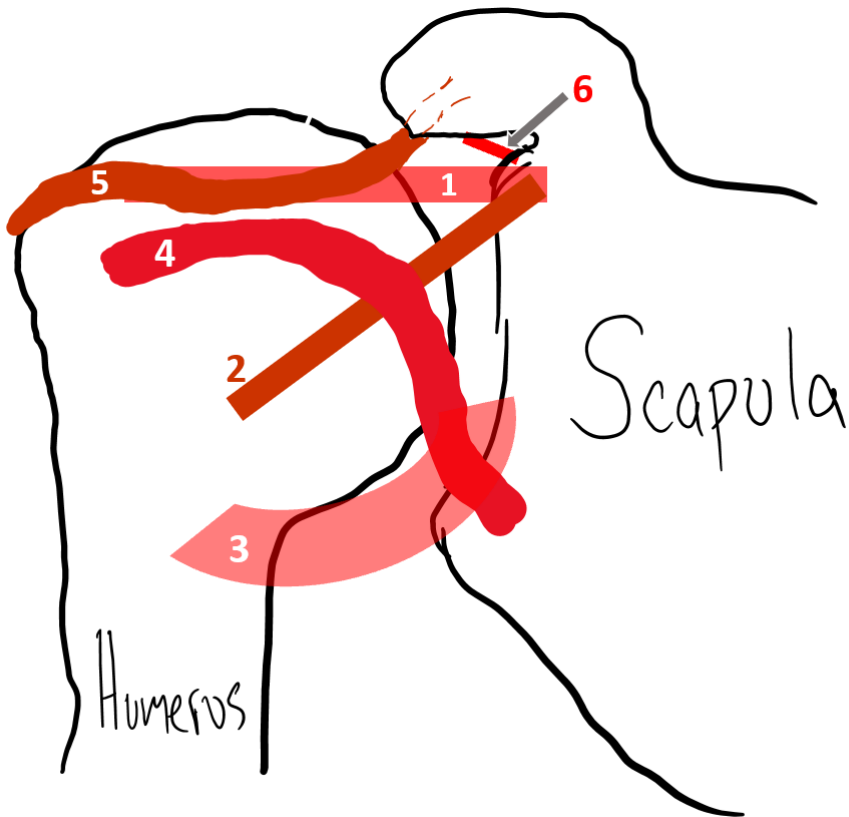


Table Glenohumeral Ligaments

	Component	Scapula Attachments	Humeral Attachments
1	Superior Glenohumeral Ligament	Supraglenoid tubercle of the scapula	Proximal tip of the lesser tuberosity on medial ridge
2	Middle Glenohumeral Ligament	anterosuperior glenoid	Anterior aspect of the proximal humerus
3	Inferior Glenohumeral	inferior two-thirds of the glenoid labrum and/or neck	Inferior aspect of the anatomical humeral neck

	ligament (anterior, posterior, inferior)		
4	Spiral Ligament	Infraglenoid tubercle	Lesser tubercle with subscapularis tendon
5	Coracohumeral	Lateral border of coracoid process	Greater tubercle of the humerus
6	Coracoglenoid	Coracoid process between the coracoacromial and coracohumeral ligaments Supraglenoid tubercle covering the origin of the long tendon of the biceps	NA

Appendix C: Potential Soft Tissue Material Options

Material	Use	Unit/Cost	Pros	Cons
Urethane	Tendons & ligaments	~\$35/2lbs	Reynold's Advanced Materials This material was discussed with Dr. Crispin P. Weinberg during our interview due to its high	Creates toxic by product Not currently Available for manufacturing at WPI

			<p>stiffness and large range of other material properties</p> <p>70 Shore D Cast Urethane-</p> <p>TS: 45 MPa</p>	
<p>PFTE-</p> <p>Polytetrafluoroethylene</p>	Tendons & ligaments	\$4.99/lb.	<p>Fibers are used to make a replacement artificial ligament for anterior cruciate ligament</p>	Difficult to manufacture
<p>PET-</p> <p>Polyethylene terephthalate (Teflon)</p>	Tendons & ligaments		<p>EM: 3.5-11GPa</p> <p>TS:60-140MPa</p> <p>Fibers are used to make a replacement artificial ligament for anterior cruciate ligament for people</p>	Difficult to manufacture
<p>Nylon, PA-</p> <p>Polyamide</p>	Tendons & ligaments	\$24.95/roll	<p>EM: 1.1-16GPa</p> <p>TS:35-210MPA</p> <p>Commonly available in varying braiding patterns and structure creating different material behavior</p>	<p>A low coefficient of friction could present issues tying knots, however other methods of attachments can be utilized such as bonding agents or mechanical fasteners</p>

			<p>Low coefficient of friction</p> <p>Is a current material being developed for ligament replacement</p>	
PLA	Ligament	\$62.5/1L	<p>EM: 3.5GPa/SM: 1.28GPa</p> <p>TS: 59MPa</p> <p>Readily accessible</p> <p>Team has experience working with this in 3D printing and related software</p>	<p>Difficult to model intricate curves of ligament attachments</p> <p>3D prints may also be too brittle at the thicknesses needed</p>
Mold Star 30- Silicone rubber	Muscles	~\$11.50/1 lb	<p>EM: 420 psi SM 96 psi 339%</p> <p>Available at Reynold's Adv. Materials</p>	Tensile strength much higher than natural muscle
Eco Flex-Silicone rubber	Muscles	~\$33/2lbs	<p>\$33 for 2lbs at</p> <p>Available at Reynold's Advanced Materials</p> <p>120 psi 8 psi 800%</p> <p>Has been studied to show similar stress</p>	<p>More complex material properties than linear elastic bands that behave predictably with differing force loads, whereas this silicone rubber has</p>

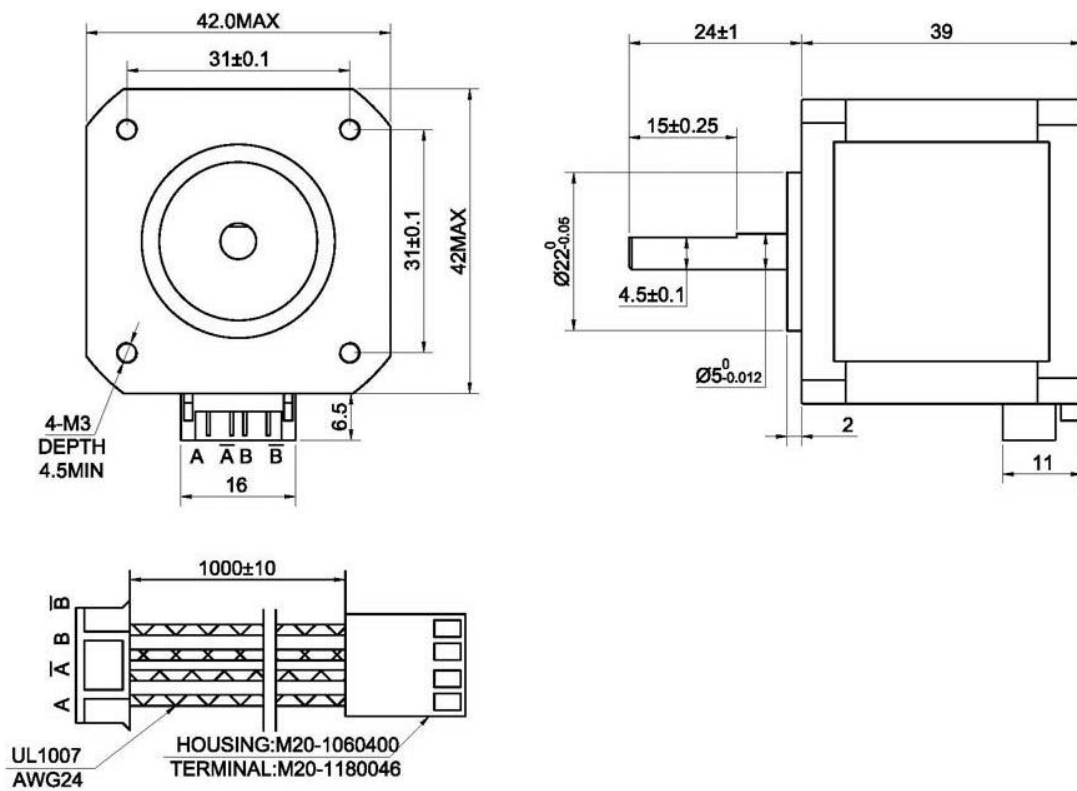
		<p>distributions as muscle</p> <p>Twice the normal tensile strength of muscle</p> <p>Provides more dynamic material properties under loading than traditional elastic bands with more linear behavior</p> <p>Indentation tests showed similar stress distribution trends in muscle and Ecoflex 0030</p> <p>Stress magnitudes were higher in Eco flex 0030 than in porcine muscle. All 3 silicone formulations demonstrated shear moduli within the range of published values for biological tissue. For the experimental</p>	<p>viscoelastic properties making force and elastic properties realistically difficult.</p> <p>Concerns about high coefficients of friction with rubber material due to the overlapping and strains that need to occur for multiple muscles.</p>
--	--	--	--

			<p>conditions reported in this work, Ecoflex 0030 exhibited greater stiffness than porcine (pig) muscle which is similar to muscles of humans</p>	
Natural Latex	Muscles	\$10/	<p>Precut affordable bands that are traditionally used to exercise and rehabilitate muscles</p> <p>Team members have access to resources as well as traditional online websites that have a large assortment of resistance bands with varied sizes, resistances, and thickness.</p> <p>Will use to prototype initial design iterations as the many differing properties can be layered to</p>	<p>Concerns about high coefficients of friction with rubber material due to the overlapping and strains that need to occur for multiple muscles.</p>

			create more complex results.	
--	--	--	------------------------------	--

Appendix D: Stepper Motor Specifications

NEMA 17 Stepper Motor Specifications



Manufacturer Part Number:	17HS15-1504S-X1
Motor Type	Bipolar Stepper
Step Angle	1.8 deg
Holding Torque	45Ncm(63.74oz.in)

Rated Current/phase	1.50A
Phase Resistance	2.3ohms
Inductance	4.4mH ± 20%(1KHz)
Driving Voltage	12-24VDC

NEMA 17 Planetary Motor Specifications

Nema 17 Planetary Geared Stepper Motor

Rev: A

Date:

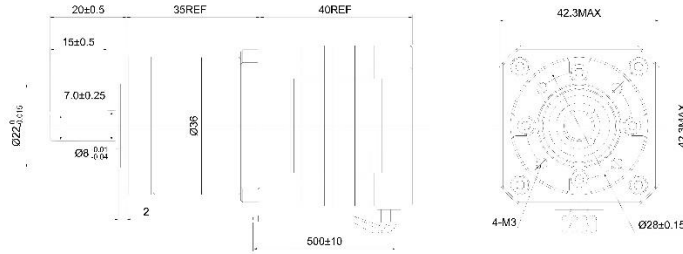
COMMON RATINGS

Step angle : 1.8° Dielectric strength : 500VAC
 Positional accuracy : ±5% Insulation resistance : 100Mohm(500VDC)
 Number of Phase : 2 Ambient Temperature : -10°C~50°C
 Temperature rise : 80°C MAX Insulation class : B
 Rotor Inertia : 54gcm² Weight : 0.55Kg

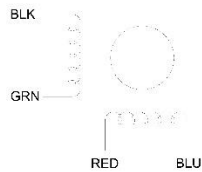
SPECIFICATIONS

Holding Torque Before Gearbox (N.cm)	Rated Current/Phase (Amps DC)	Phase Resistance (ohms) ±10%	Rated Voltage/Phase (V DC)	Phase Inductance (mH) ±20%(1KHz) Typical
36.0	1.68	1.65	2.8	3.2

DIMENSIONS unit=mm



CONNECTIONS



GEARBOX

Gear Ratio 26
 Efficiency 81%
 Backlash at No-load <= 1°
 Max. Permissible Torque(Nm) 3.0
 Moment Permissible Torque(Nm) 5.0
 Shaft Maximum Axial Load(N) 50.0
 Shaft Maximum Radial Load(N) 100.0

17HS15-1684S-PG27					技术规格书	
标记	处数	分区	更改文件号	签名	日期	
设计			标准化			
审核						www.OMC-StepperOnline.com
工艺			批准			

References

3D Printed Medical Models – State of the Art 2021. (2021, April 15). All3DP Pro.

<https://all3dp.com/1/3d-printed-medical-models/>

3D Printing in the Hospital. (n.d.). Retrieved September 16, 2021, from

<https://3d.formlabs.com/white-paper-3d-printing-in-the-hospital/>

Anatomical Models | Human Joint Models | Deluxe Functional Shoulder Joint Model. (n.d.).

Retrieved September 16, 2021, from https://www.a3bs.com/deluxe-functional-human-shoulder-joint-physiological-movable-3b-smart-anatomy-1000160-a801-3b-scientific_p_35_157.html?searchinput=shoulder&searchword=shoulder

Anatomy of the Shoulder. (2019, April 9). UT Health San Antonio.

<https://www.uthscsa.edu/patient-care/physicians/sports-medicine/shoulder-anatomy>

Anatomy—Musculoskeletal Ultrasonography. (n.d.). Retrieved September 15, 2021, from

<https://sites.google.com/site/honkichoi/shoulder/anatomy>

Asadi Nikooyan, A., Veeger, H. E. J., Chadwick, E. K. J., Praagman, M., & van der Helm, F. C.

T. (2011). Development of a comprehensive musculoskeletal model of the shoulder and elbow.

Medical & Biological Engineering & Computing, 49(12), 1425–1435.

<https://doi.org/10.1007/s11517-011-0839-7>

Bednarski, R., Bielak, A., & Wojciechowski, A. (2019). Review of muscle modelling methods

from the point of view of motion biomechanics with particular emphasis on the shoulder. *Open*

Physics, 17(1), 545–555. <https://doi.org/10.1515/phys-2019-0056>

Behrmann, G. P., Hidler, J., & Mirotznik, M. S. (2012). Fiber optic micro sensor for the measurement of tendon forces. *BioMedical Engineering OnLine*, 11, 77.

<https://doi.org/10.1186/1475-925X-11-77>

Biomechanics of the shoulder and elbow | Elsevier Enhanced Reader. (n.d.). Retrieved

September 15, 2021, from

<https://reader.elsevier.com/reader/sd/pii/S1877132717300799?token=8CA899DB10666F12688F90AC8B19166311CB63A92D1583BB078BC9883E62D9E6794D5FE38E6EAFE7C76CCA92BA94C8D7&originRegion=us-east-1&originCreation=20210915171217>

Bishop, J. Y., & Kaeding, C. (2006). Treatment of the Acute Traumatic Acromioclavicular Separation. *Sports Medicine and Arthroscopy Review*, 14(4), 237–245.

<https://doi.org/10.1097/01.jsa.0000212330.32969.6e>

Bolsterlee, B., Veeger, D. H. E. J., & Chadwick, E. K. (2013). Clinical applications of musculoskeletal modelling for the shoulder and upper limb. *Medical & Biological Engineering & Computing*, 51(9), 953–963. <https://doi.org/10.1007/s11517-013-1099-5>

Bones & Joints of the Shoulder | ShoulderDoc. (n.d.). Retrieved September 15, 2021, from <https://www.shoulderdoc.co.uk/article/1177>

Broken collarbone—Symptoms and causes. (n.d.). Mayo Clinic. Retrieved September 12, 2021, from <https://www.mayoclinic.org/diseases-conditions/broken-collarbone/symptoms-causes/syc-20370311>

Brophy, R. H., Barnes, R., Rodeo, S. A., & Warren, R. F. (2007). Prevalence of musculoskeletal disorders at the NFL Combine—Trends from 1987 to 2000. *Medicine and Science in Sports and Exercise*, 39(1), 22–27. <https://doi.org/10.1249/01.mss.0000241637.52231.18>

Bull, A. M. J., Reilly, P., Wallace, A. L., Amis, A. A., & Emery, R. J. H. (2005). A novel technique to measure active tendon forces: Application to the subscapularis tendon. *Knee Surgery, Sports Traumatology, Arthroscopy: Official Journal of the ESSKA*, 13(2), 145–150. <https://doi.org/10.1007/s00167-004-0556-y>

Clouthier, A., Hetzler, M., Fedorak, G., Bryant, J., Deluzio, K., & Bicknell, R. (2015, April 29). *Effect of Loading Direction on Force to Dislocate in Reverse Shoulder Arthroplasty*.

Crim, J. R. (Ed.). (2018). Shoulder Anatomy. In *Specialty Imaging: Arthrography (Second Edition)* (pp. 42–57). Elsevier. <https://doi.org/10.1016/B978-0-323-59489-9.50017-8>

Ekstrand, J., Hägglund, M., Törnqvist, H., Kristenson, K., Bengtsson, H., Magnusson, H., & Waldén, M. (2013). Upper extremity injuries in male elite football players. *Knee Surgery, Sports*

Traumatology, Arthroscopy: Official Journal of the ESSKA, 21(7), 1626–1632.

<https://doi.org/10.1007/s00167-012-2164-6>

Enger, M., Skjaker, S. A., Nordsletten, L., Pripp, A. H., Melhuus, K., Moosmayer, S., & Brox, J. I. (2019). Sports-related acute shoulder injuries in an urban population. *BMJ Open Sport — Exercise Medicine*, 5(1), e000551. <https://doi.org/10.1136/bmjsem-2019-000551>

Feel the difference. Stratasys J750™ Digital Anatomy™ 3D Printer. (n.d.). Stratasys. Retrieved September 16, 2021, from <https://www.stratasys.com/3d-printers/j750-digital-anatomy>

Go from Scan to 3D Model | Materialise Mimics InPrint. (n.d.). Retrieved September 16, 2021, from <https://www.materialise.com/en/medical/software/materialise-mimics-inprint>

Gorbaty, J. D., Hsu, J. E., & Gee, A. O. (2017). Classifications in Brief: Rockwood Classification of Acromioclavicular Joint Separations. *Clinical Orthopaedics and Related Research*, 475(1), 283–287. <https://doi.org/10.1007/s11999-016-5079-6>

Halder, A. M., Kuhl, S. G., Zobitz, M. E., Larson, D., & An, K. N. (2001). Effects of the Glenoid Labrum and Glenohumeral Abduction on Stability of the Shoulder Joint Through Concavity-Compression: An: in Vitro: Study. *JBJS*, 83(7), 1062–1069.

Hamroongroj, T., Tantikul, C., & Keatkor, S. (2000). The clavicular fracture: A biomechanical study of the mechanism of clavicular fracture and modes of the fracture. *Journal of the Medical Association of Thailand = Chotmaihet Thangphaet*, 83(6), 663–667.

Kaplan, L. D., Flanigan, D. C., Norwig, J., Jost, P., & Bradley, J. (2005). Prevalence and variance of shoulder injuries in elite collegiate football players. *The American Journal of Sports Medicine*, 33(8), 1142–1146. <https://doi.org/10.1177/0363546505274718>

Kiel, J., & Kaiser, K. (2021). Acromioclavicular Joint Injury. In *StatPearls*. StatPearls Publishing. <http://www.ncbi.nlm.nih.gov/books/NBK493188/>

Koh, S.-W., Cavanaugh, J. M., & Leach, J. P. (n.d.). Mechanical Properties of the Shoulder Ligaments Under Quasi-static and Dynamic Loading. 1.

Li, K. (2016). Review of the Strain Modulation Methods Used in Fiber Bragg Grating Sensors. *Journal of Sensors*, 2016, e1284520. <https://doi.org/10.1155/2016/1284520>

Marom, N., & Williams III, R. (2018). Upper Extremity Injuries in Soccer. *American Journal of Orthopedics*, 47. <https://doi.org/10.12788/ajo.2018.0091>

Mimics inPrint & Formlabs | Materialise. (n.d.). Retrieved September 16, 2021, from <https://www.materialise.com/en/medical/mimics-inprint-formlabs>

Monash 3D printing—Monash Biomedicine Discovery Institute. (n.d.). Retrieved September 16, 2021, from <https://www.monash.edu/discovery-institute/chaes/services-and-facilities/monash-3d-printing>

Muscles of Shoulder Region | Bone and Spine. (n.d.). Retrieved September 15, 2021, from <https://boneandspine.com/muscles-of-shoulder/>

Poeggel, S., Tosi, D., Duraibabu, D., Leen, G., McGrath, D., & Lewis, E. (2015). Optical Fibre Pressure Sensors in Medical Applications. *Sensors (Basel, Switzerland)*, 15(7), 17115–17148. <https://doi.org/10.3390/s150717115>

Range-of-motion-exercises-for-shoulder. (n.d.). *Post Competitive Insight*. Retrieved September 15, 2021, from <https://postcompetitiveinsight.com/wp-content/uploads/2015/10/range-of-motion-exercises-for-shoulder.jpg>

Saw, R., Finch, C. F., Samra, D., Baquie, P., Cardoso, T., Hope, D., & Orchard, J. W. (2017). Injuries in Australian Rules Football: An Overview of Injury Rates, Patterns, and Mechanisms Across All Levels of Play. *Sports Health*, 10(3), 208–216. <https://doi.org/10.1177/1941738117726070>

Seth, A., Matias, R., Veloso, A. P., & Delp, S. L. (2016). A Biomechanical Model of the Scapulothoracic Joint to Accurately Capture Scapular Kinematics during Shoulder Movements. *PLoS ONE*, 11(1), e0141028. <https://doi.org/10.1371/journal.pone.0141028>

Shoulder Anatomy. (n.d.). Retrieved September 12, 2021, from <https://anatomy.lexmedicus.com.au/collection/shoulder>

SLAP Tears—OrthoInfo—AAOS. (n.d.). Retrieved September 12, 2021, from <https://www.orthoinfo.org/en/diseases--conditions/slap-tears/>

SOMS Functional Anatomy Model Of The Shoulder Joint. (n.d.). Anatomy Warehouse. Retrieved September 16, 2021, from <https://anatomywarehouse.com/functional-anatomy-model-of-the-shoulder-joint-a-102696>

Sopakayang, R. (2010). *Viscoelastic Models for Ligaments and Tendons*. <https://vtechworks.lib.vt.edu/handle/10919/77298>

Special Issue on Rotator Cuff Biology and He. (n.d.).

Stefko, J. M., Tibone, J. E., Cawley, P. W., ElAttrache, N. E., & McMahon, P. J. (n.d.). Strain of the anterior band of the inferior glenohumeral ligament during capsule failure. *Journal of Shoulder and Elbow Surgery*, 6(5), 473–479.

Sun, W., Starly, B., Nam, J., & Darling, A. (2005). Bio-CAD modeling and its applications in computer-aided tissue engineering. *Computer-Aided Design*, 37(11), 1097–1114. <https://doi.org/10.1016/j.cad.2005.02.002>

Varacallo, M., Musto, M. A., & Mair, S. D. (2021). Anterior Shoulder Instability. In *StatPearls*. StatPearls Publishing. <http://www.ncbi.nlm.nih.gov/books/NBK538234/>

Yang, J., Feng, X., Kim, J., & Rajulu, S. (2010). Review of biomechanical models for human shoulder complex. *Int. J. of Human Factors Modelling and Simulation*, 1, 271–293. <https://doi.org/10.1504/IJHFMS.2010.036791>

Zens, M., Ruhhammer, J., Goldschmidtboeing, F., Woias, P., Feucht, M., Mayr, H., & Niemeier, P. (2014). A New Approach to Determine Ligament Strain Using PDMS Strain Gauges: Exemplary Measurements of the Anterolateral Ligament. *Journal of Biomechanical Engineering*. <https://doi.org/10.1115/1.4028837>

Zhang, Q., Adam, N. C., Hosseini Nasab, S. H., Taylor, W. R., & Smith, C. R. (2021). Techniques for In Vivo Measurement of Ligament and Tendon Strain: A Review. *Annals of Biomedical Engineering*, 49(1), 7–28. <https://doi.org/10.1007/s10439-020-02635-5>